Surface-Functionalized Layered Double Hydroxides (LDHs) Nanoplatelets for Enhanced Thermal Stability of Plasticized Polyvinyl Chloride (PVC) films

Hossein Ipakchi[1], Kushal Panchal[2], Roozbeh Mafi[1], and Li Xi[1]*

[1]Department of Chemical Engineering, McMaster University, Hamilton, Ontario, L8S 4L7, Canada.

[2]Oligomaster Inc., Hamilton, Ontario, L8P 0A1, Canada.

*Corresponding author: xili@mcmaster.ca

Abstract

Surface and interfacial engineering of additives is crucial for enhancing the compatibility between inorganic additives and polymer matrices. Thermal stabilizers are particularly prevalent in polyvinyl chloride (PVC) compounding. Recently, layered double hydroxidehydroxide (LDH) structures have been explored as a new class of efficient and environmentally-friendly stabilizers. This study uses oleic acid (OA) as a bio-sourced surface-active agent for improved compatibility between MgAlZn-CO_3 LDH and the PVC matrix. Scanning electron microscopy (SEM) results indicated that OA substantially influences the distribution of LDHs throughout PVC matrix. Additionally, Raman spectroscopy confirmed that the incorporation of OA enhances the HCl absorption capability of LDHs, leading to an over two-fold increase in the static thermal stability of PVC. Correspondingly, color stability of PVC compounds with the modified LDH also improves significantly. The surface-functionalized LDH developed in this work exhibits tremendous potential as a highly potent and yet environmentally-friendly stabilizer for PVC processing as well as for PVC recycling and its circular economy.

Keywords: Layered Double Hydroxide, Heating Stabilizer, PVC compounds, Oleic Acid, Sustainable additives, Surface Functionalization

1. Introduction

Polyvinyl chloride (PVC) is one of the oldest commercial thermoplastics and also one of the most widely-used , following polyethylene (PE) and polypropylene (PP)[1]. PVC resin offers a wide range of advantages, including oil and grease resistance[2], good fire retardancy[3], and versatility in packaging[4]. It is widely used in various applications such as construction [5], and healthcare[6] applications. However, PVC plastics suffer from low thermal and UV stability. Weak thermal stability arises from defects in the PVC structures, such as allyl chloride, tertiary chloride, and head-to-head arrangements. During thermal degradation, carbon-carbon bonds form, and hydrochloric acid (HCl) is released as a side product. The latter acts as a catalyst and accelerates the degradation of PVC. This process is known as autocatalytic dehydrochlorination degradation of PVC resin[7].

To address this issue, a wide range of thermal stabilizers have been used in PVC resin formulation[8] such as Calcium/Zinc (Ca/Zn), Barium/Zinc (Ba/Zn), etc. These additives serve to intercept hydrochloride from PVC decomposition, which prevents further degradation of the material. However, it's essential to recognize that these chemicals, which often take the form of complex compounds containing heavy metals, such as cadmium, barium, and lead, come with their own set of challenges. Specifically, their toxicity poses increasing concerns for health and environmental reasons. Lead, in particular, is highly toxic, which prompted regulatory actions[9]. The RoHS directive, issued in 2003, and the REACH regulation implemented by the European Union (EU) in 2007 strictly control the use of lead salts. In the field of PVC, organizations like ESPA (European Stabiliser Producers Association), together with VinylPlus Voluntary Commitment and EuPC (European Plastics Converters), have committed to replacing lead-based stabilizers. By the end of 2015, the use of lead salts was banned in the EU[10].

PVC consumption in industrial applications is anticipated to reach 65 million tons by 2030 [11], which has heightened the demand for environmentally friendly heat stabilizers. Layered Double Hydroxide (LDH) emerges as a promising candidate for this purpose. LDHs conform to the general chemical formula: $[M^{(II)}_{1-x}\ M^{(III)}_{x}\ (OH)_2]^{+}\ (An)^{n-}_{x/n}\ mH_2O$. In this expression, $M^{(II)}$ and $M^{(III)}$ denote divalent and trivalent metal cations, respectively. The viable divalent and trivalent cations for LDH synthesis include Mg^{2+}, Ca^{2+}, Ni^{2+}, Cu^{2+}, Zn^{2+}, Al^{3+}, Fe^{3+}, Cr^{3+}, Ga^{3+}, and Mn^{3+}. The An^{-} symbolizes the anion within the interlayer gallery, including NO_3^{-}, CO_3^{2-}, Cl^{-}, and SO_3^{2-}[12].

Research findings have shown that LDHs have the capability to absorb and neutralize hydrochloric acid (HCl) generated during the degradation process of PVC. This impedes the catalytic influence of HCl on PVC degradation [13]. Several key parameters influence LDHs' efficiency as heat stabilizers, including the type and composition of the underlying metal ions, the anions present in the interlayer gallery, the synthesis methodology, and functional characteristics[14]. Notably, varying the magnesium (Mg) to aluminum (Al) ratio in LDHs reveals a spectrum of thermal stability for PVC, with the Mg/Al ratio of 2 yielding optimal enhancement. By increasing the Mg/Al ratio, electrostatic attraction between the basic metal and interlayer anions diminishes, which reduces the driving force for Cl^- absorption into the interlayer[15]. Furthermore, the choice of anions within the interlayer gallery significantly impacts LDHs' efficiency, particularly through ion exchange processes during HCl absorption. While CO_3^{2-} remains a common anion for interlayer applications in PVC heat stabilization, researchers have explored multifunctional anions with greater capacity[16]. Examples include 2-hydroxy-4-methoxybenzophenone-5-sulfonate anion (BP^-)[17], dipentaerythritol (Dpe)[18], meta-phosphoric acid (HPO_3)[19], and stearic groups[13]. These alternatives increase the interlayer spacing, which weakens hydrogen bonds between hydroxyl groups and the basic layers, thereby enhancing the hydroxyl groups' activity in HCl absorption.

The compatibility between LDH and the polymer matrix is a crucial parameter in the application of LDH as a thermal stabilizer. The optimization of compound properties is greatly influenced by the uniform distribution of additives within the polymer matrix[20]. However, owing to its inorganic composition, LDH tends to agglomerate within PVC. As a result, surface modification with an organic structure becomes necessary. Research demonstrated that employing the stearate group as an LDH surface modifier enhances the thermal stability of PVC compounds by 20 times more compared to pure compounds[21]. Additionally, LDH distribution within PVC significantly improves. PVC compounds incorporating Polyethylene glycol (PEG)-LDH-epoxy soybean oil as a thermal stabilizer exhibit structural stability against thermal degradation and maintain color integrity even after 120 minutes at 180°C[22]. Other organic compounds used for LDH surface modification include Dodecyl sulfate[21], Alkyl phosphonate[23], Toluene-2,4-di-isocyanate (TDI)[24], and PEG[22].

Oleic Acid (cis-9-octadecenoic acid) (OA), an environmentally friendly fatty acid, constitutes 55-80% of olive oil and 15-20% of grape seed oil[25]. There has been an increasing emphasis on the utilization of OA as a sustainable additive in the production of PVC, particularly as plasticizers and lubricants. Research findings indicated that employing OA as the principal source of bio-based plasticizers not only mitigates plasticizer migration but also improves the thermal and color stability of plasticized PVC compounds when compared to commercial plasticizers such as dioctyl

terephthalate (DOTP). To the best of our knowledge, OA has not been previously utilized as a surface modifier for LDH in thermal stabilizer applications within PVC compounds. Here, we select OA as a new surface modifier for several reasons. First, it is an organic molecule acknowledged for its sustainability and environmental compatibility, which aligns with the contemporary trend toward greener chemical processes. Second, its long aliphatic chain and the structure of its unsaturated bonds render it a promising candidate for integration into plasticized polymers, thereby offering compatibility and enhanced interfacial adhesion between the LDH and PVC. In addition, OA is a liquid at room temperature, which facilitates its synthesis and surface modification procedures. This is a clear advantage over solid fatty acids, like stearic acid, which have also been investigated in the literature for their efficacy in polymer stabilization[26]. Moreover, the unsaturated bonds present in OA provide the potential for additional interactions within the PVC matrix, potentially enhancing the overall stabilization mechanism.

The goal of this study is to investigate the potential of OA as an agent for the surface functionalization of LDH for its improved dispersion in the PVC matrix and thermal stabilization effectiveness. This study synthesize MgAlZn-CO_3 layered double hydroxide (LDH) using the coprecipitation method, which was widely used for LDH preparation in thermal stabilizer applications. Various Mg/Zn molar ratios are used to test the optimal value. The impact of LDH compositions on the thermal stability of PVC is investigated. In the subsequent stage, the surface of the most promising LDH nanoparticles underwent modification using OA as the surface modifier agent. Performance of the surface (OA)-modified LDH is compared with the original LDH. The role of OA in the improvement of thermal stability is also studied.

2. Materials and Methods

2.1.Chemicals and Materials

Zinc nitrate hexahydrate ($Zn(NO_3)_2 \cdot 6H_2O$), magnesium nitrate hexahydrate ($Mg(NO_3)_2 \cdot 6H_2O$), and aluminum nitrate nonahydrate ($Al(NO_3)_3 \cdot 9H_2O$) were obtained as analytical reagents (AR) with a purity greater than 99.0% from Sigma Aldrich. Sodium hydroxide (NaOH, AR, >96.0%) and sodium carbonate (Na_2CO_3, AR, >99.5%) were also purchased from Sigma Aldrich. OA, ($CH_3(CH_2)_7CH=CH(CH_2)_7COOH$), was sourced from the same supplier. The PVC resin suspension (grade K=70) was supplied by ShinTech Inc, while diisononyl phthalate (DINP, $C_{26}H_{42}O_4$) and the calcium/zinc thermal stabilizer came from Evonik Oxeno LLC and AM Stabilizers, respectively.

2.2.Methods

2.2.1. Synthesis of LDH-derivatives

To synthesize LDHs, three different metal compositions were considered. The Mg/Zn ratio, denoted as 'R,' varied at 0.5, 1, and 2 (detailed in Table S-1). Initially, the metal hexahydrates were dissolved in 500 mL of deionized water (referred to as solution A). The precipitant solution (solution B) consisted of 1 mol/L NaOH and 0.1 mol/L Na_2CO_3 blended in 100 mL of deionized water. Next, 100 mL of deionized water was added to a three-necked flask, followed by the addition of solution A, which was vigorously stirred. Solution B was then gradually added dropwise at 80°C, maintaining the solution pH at 11±0.1 throughout the reaction. The resulting precipitate was incubated at 80°C for 24 hours under a nitrogen atmosphere and subsequently centrifuged three times using a mixture of deionized water and ethanol (1:1). Finally, the thick slurry solution was vacuum-dried for 18 hours at 60°C until a white powder was obtained. A schematic of the procedure is shown in Figure 1-a. Before synthesizing ternary LDHs (used in this study), binary MgAl-LDH and ZnAl-LDH structures were first synthesized for comparison with the commercial sample C-915 provided by Clarient Specialty Chemicals. As shown in Table S-2 and Figure S-1, our binary LDHs display highly similar structural features as the commercial sample, which confirmed the correctness of our synthesis procedure.

2.2.2. LDH surface modification

In their study, Obata et al.[27] investigated sodium oleate (SOA)/Mg–Al–SO_4–LDH systems for drug delivery applications. When the SOA/LDH concentration was ≤5 mM, the SOA group modified the LDH surface without ion exchange. However, for SOA/LDH concentrations ≥10 mM, SOA penetrated between the layers, leading to ion exchange. Interestingly, there is no available information for SOA/LDH concentrations between 5 and 10 mM. To address this gap, we explored OA/LDH ratios of 3, 6, 9, and 12 mM. These samples are labeled with LDH-3OA, LDH-6OA, LDH-9OA and LDH-12OA, respectively, with detailed formulations listed in Table S-3. The surface-modified LDHs were prepared as follows: Methanol and OA were mixed under stirring, and MgZnAl-CO_3 LDHs were added. The temperature was maintained at 70°C for 24 hours, followed by centrifugation and drying, similar to the previous steps as shown in Figure 1-b.

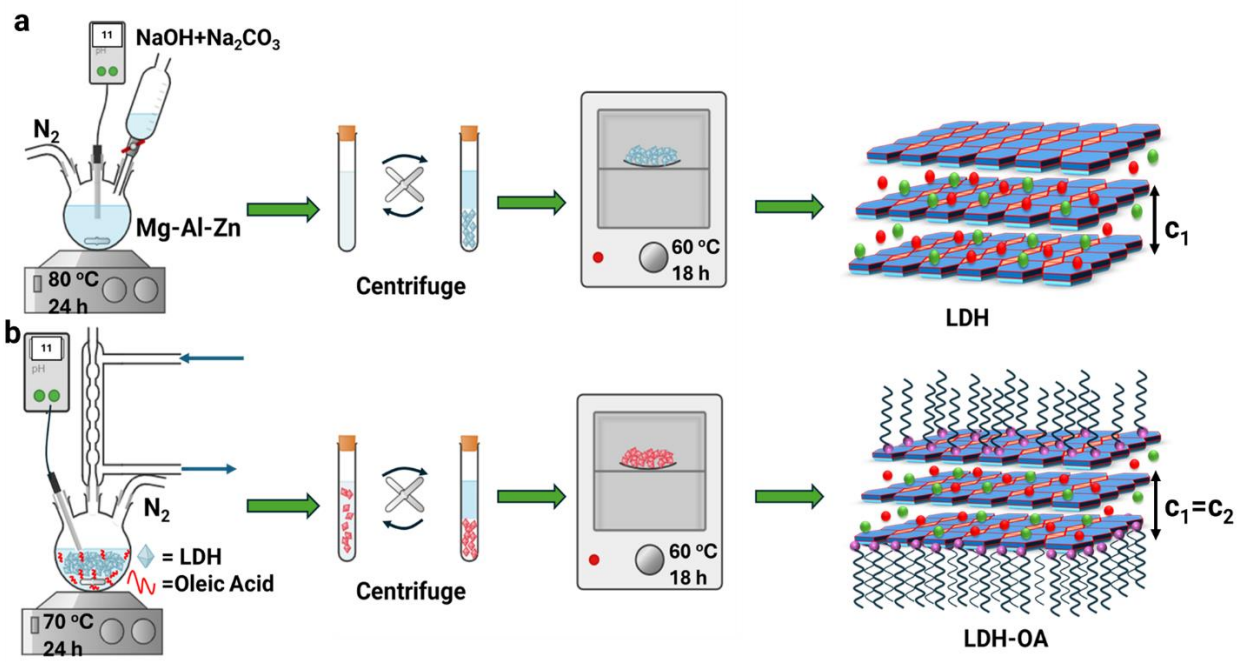

Figure 1 Schematic of LDH a) synthesis and b) surface modification procedures.

2.2.3. Preparation of PVC-compounds

All PVC blends contain 45 phr (parts per hundred resin – i.e., on the basis of 100 parts of PVC by weight) DINP, 2.5 phr Ca/Zn thermal stabilizer, and varying amount/type of LDHs, according to the formulations reported in Table S-4. The ingredients were first mixed into a dry blend which then underwent melt mixing under identical conditions: a temperature of 150°C and a torque of 50 rpm for 7 minutes using a batch mixer. After compounding, the plasticized PVC sheets were prepared via compression molding. The process involved maintaining the compounded mixture at 150°C for 5 minutes as a preheating step, followed by applying a pressure of 10 MPa for an additional 5 minutes. Images of the plasticized PVC sheets are presented in Figure S-2.

3. Material characterization

3.1. LDH characterization

3.1.1. Structural Analysis

The crystallinity of the synthesized LDH was determined through powder X-ray diffraction (PXRD) analysis conducted at the McMaster Analytical X-Ray Diffraction Facility (MAX). Cu Kα radiation (λ = 0.154 nm) was employed within a 2θ range from 5° to 80°. Additionally, the infrared spectra were acquired using a Thermo Scientific Nicolet 6700 FT-IR Spectrophotometer, covering the wavenumber range of 4000–400 cm^{-1}. The powder sample was mixed with KBr and pressed into pellets. The FTIR spectra were collected with 64 scans and a resolution of 1 cm^{-1}.

3.1.2. Textural and Morphological Analysis

The specific surface area (SSA) and pore size distribution measurements were conducted using a Quantachrome ASiQwin instrument. Nitrogen gas (N_2) served as the adsorbate at 77 K. The Brunauer-Emmett-Teller (BET) method was employed to determine the surface area through a multipoint approach, while the Barrett-Joyner-Halenda (BJH) desorption method was utilized to calculate the pore size distribution. Before analysis, samples were degassed at 120 °C for 12 hours to remove any adsorbed species. Additionally, the surface morphology of the LDH was investigated using scanning electron microscopy (SEM) with an FEI Magellan 400 instrument, operating at an accelerating voltage of 1-2 kV. LDH suspensions in water were deposited onto a holder, affixed to a platinum-coated grid, and imaged after natural drying at room temperature.

3.1.3. Surface and Compositional Analysis

X-ray photoelectron spectroscopy (XPS) analyses were conducted using a PHI Quantera II scanning XPS microprobe (Physical Electronics, USA). High-resolution scans were performed for the C 1s, O 1s, Zn 2P ($2P_{3/2}$ and $2P_{1/2}$), Al 2P, and Mg 1S regions. Peak fitting for the C 1s, O 1s, Zn 2P ($2P_{3/2}$ and $2P_{1/2}$), Al 2P, and Mg 1S peaks involved Gaussian functions after background subtraction. Additionally, inductively coupled plasma−atomic emission spectroscopy (ICP-AES) was employed to determine the metal elemental composition.

3.1.4. Thermal Analysis

The thermal gravimetric analysis (TGA) thermograms were obtained during the heating process using a Thermo Gravimetric Analyzer (TA Q50) under a nitrogen gas atmosphere. The heating rate was set at 10 °C/min, ranging from room temperature to 700°C.

3.2.PVC compounds characterization

3.2.1. Structural and Morphological Analysis

Raman spectroscopic measurements were conducted using a Renishaw InVia spectrometer equipped with an Ar ion laser (532 nm and 785 nm, power 50 mW), a Leica DMLM confocal microscope, and a CCD detector. The Raman spectra were recorded using 5% of the laser power, covering the spectral range of 200–4000 cm^{-1} with a resolution of 3 cm^{-1}. Three data points were collected for each investigated sample. Additionally, FT-IR was employed to study PVC sheets, covering the wavenumber range of 4000–400 cm^{-1}. Furthermore, to investigate the morphology and compatibility of LDHs with PVC, SEM and energy-dispersive spectroscopy (EDS) analysis of SEM micrographs were performed.

3.2.2. *Thermal stability of PVC compounds*

To determine the static thermal stability (STS) properties of PVC compounds, we employed Congo Red (ISO 182-1, 1990), dehydrochlorination (ISO 182-2: 1990-12), discoloration (ISO 305-4, 1990), and TGA methods.

In the Congo Red test, a PVC sample was placed in a closed test tube, and a strip of Congo Red paper was positioned at the top of the tube. The color change was observed when the test tube was immersed in an oil bath at 180°C. For the discoloration test, PVC films (cut to 10×10 mm with a 1 mm thickness) were heated in an oven at 180°C, and the color change was monitored every 10 minutes. Changes in color parameters (*ΔL, ΔA*, and *ΔB*) were obtained using a VEYKOLOR Pro color meter and $\Delta \boldsymbol{E}$ calculated by Equation 1:

$$\Delta \boldsymbol{E} = \sqrt{\Delta \boldsymbol{L}^2 + \Delta \boldsymbol{A}^2 + \Delta \boldsymbol{B}^2}. \qquad (1)$$

ΔL, ΔA, and *ΔB* values represent the changes in sample color, compared with the unaged sample, in white (+) vs. black (-), red (+) vs. green (-), and yellow (+) vs. blue (-) scales, respectively. For example, PVC degradation is often signified by the yellowing of the sample, which is reflected in a positive *ΔB* value, while a low *ΔE* value indicates small over-all color difference from the original sample. Thus, *ΔE* and *ΔB* values are chosen as the main indicators for the discoloration of PVC sheets Quantitative values of *ΔL*, *ΔA*, and *ΔB* are obtained using the procedure described in ASTM D2244-22.

In the dehydrochlorination test, 2 grams of PVC compounds were placed in a test tube within an oil bath at 180°C (Figure S-3). The released HCl gas in the test tube was carried by N_2 gas to 100 ml of deionized water at room temperature. The conductivity of the water was measured using a Metrohm 913 conductometer with a resolution of 0.01μS/cm. The white noise shown by the conductometer before measurements is treated as zero. TGA tests of PVC compounds used the same protocol as those used for LDHs as described in section 3.1.4.

Error bars in this work represent the standard deviation between independent replicas. Statistical differences in data were determined using one-way analysis of variance (ANOVA) with a significance level of $\alpha < 0.05$.

4. Results and Discussion

This section is organized as follows. First, in section 4.1, we will characterize the structural features of the synthesized LDHs. A comparison will be made with similar LDHs reported in the literature as well

as with commercial samples, to demonstrate the successful synthesis of LDHs with the intended structures. The effects of the Mg/Zn ratio (R) on the LDH structure will also be examined. In section 4.2, we will investigate the effects of unmodified LDHs on the stability of PVC compounds, with particular attention to the influence of the Mg/Zn ratio. LDH with the optimal Mg/Zn ratio will be used as the base material for surface modification. In section 4.3, the modified LDHs will be characterized to confirm the successful attachment of OA to LDH and examine its effects on the structure and stability of the latter. In section 4.4, we will highlight the significant improvement in PVC stability achieved using LDHs modified by OA. The effects of OA modification, its dispersion within, and its interaction with the PVC matrix will be explored. Finally, section 4.5 investigates the effect of OA-modified LDHs on PVC degradation kinetics.

4.1.Structural analysis of LDH

The powder X-ray reflection pattern of LDHs comprises two main groups: strong (003) reflections at low angles, indicating the basal spacing of LDHs. It represents the thickness of a brucite-like layer along with an interlayer. The basal spacing "c" depends on factors such as the water content between the layers, the composition of anions in the interlayer gallery, and the average charge of the metal cations[28]. This parameter is denoted as *c* and can be determined using the procedure in Gevers et al.[29]:

$$\boldsymbol{c = \frac{1}{3}(3d_{003} + 6d_{006} + 9d_{009})} \qquad (2)$$

where "*d*" represents the interlayer spacing and 2θ refers to the diffraction angle, with the subscript numbers denoting the crystal planes (*003*, *006*, *009*). The (110) position at an angle of 2θ=60° corresponds to the lattice parameter a_0 (a_0=$2d_{110}$), which represents the distance between metal-metal cations[30]. As depicted in Figure 2(a), the reflection patterns observed at specific crystallographic planes, namely (003), (006), (009), and (110), exhibit narrow widths. This observation suggests the presence of well-organized crystal lattices devoid of any impurities or accompanying by-products. The corresponding indices align with the diffraction angles illustrated in the Figure 2(a), confirming that each plane reflects X-rays at distinctive angles. This finding serves as a concrete evidence of the sample's high purity and crystallinity[29]. Additionally, the intensity of the peaks observed at the mentioned planes confirms the presence of a rhombohedral crystal lattice, which is typically expected in brucite-based structures[31].

As depicted in Table 1, the values of *c* and a_0 decrease with the increase of the Mg/Zn ratio. This is consistent with previous studies, which have shown that as the Mg/Zn ratio in $M^{II}Al$ LDHs increases,

the smaller ionic radius of Mg^{2+} (0.72 Å) compared to Zn^{2+} (0.74 Å) leads to a reduction in cation-cation distances, thereby decreasing the value of a_o under similar conditions [32]. Specifically, the equation $a_0 = \sqrt{2d(M-O)}$, where $d(M-O)$ is the metal-oxygen bond length, demonstrates the direct relationship between the radius of metal cations and a_0 [33]. Molecular dynamics simulations performed by Riahi et al. [34]have shown that Zn(II) ions exhibit distinctive solubility structures and hydration energies compared to Mg(II) ions. Consequently, the reduction in lattice parameter c with a higher Mg/Zn ratio can be attributed to the variations in hydration and ionic radii of Zn(II) and Mg(II) ions. The Zn(II) ions not only have a slightly larger ionic radius but also more favorable hydration energy, resulting in enhanced solubility and expanded interlayer spacing. The stronger interaction between Zn(II) ions and water molecules, along with the larger hydration shell surrounding Zn(II) ions, causes the layers to move further apart, thereby increasing the lattice parameter *c*. The average crystal size in (003) direction is reported in Table 1 and calculated by Scherrer's equation[15]:

$$\boldsymbol{D = \frac{0.9\,\lambda}{\beta \cos\theta}} \quad \textbf{(3)}$$

where λ is the wavelength of the X-ray used in nm, β is the full width at half maximum (FWHM-in radian) of peak (003), and θ is the Bragg diffraction angle in degree.

Table 1 Lattice parameters of unmodified LDHs.

Sample ID	2θ (003) (°)	2θ (006) (°)	2θ (009) (°)	2θ (110) (°)	d_{003}(nm)	c (nm)	a_0 (nm)	*D* (nm)
0.5R	11.526	25.226	38.726	64.546	0.767	2.169	0.306	24.017
R	11.563	25.233	38.783	60.443	0.764	2.165	0.288	23.156
2R	11.588	25.3083	38.698	60.828	0.763	2.163	0.269	23.110

The FTIR spectra of synthesized LDHs are shown in Figure 2-b. The broad peak observed between 3450-3460 cm^{-1} can be attributed to the stretching of OH groups bound to Al, Mg, and Zn ions in the layers and interlayer water molecules[35]. The strong antisymmetric vibration of CO_3^{2-} is evident at 1357-1367 cm^{-1}[36]. The weaker peak observed at around 1610-1620 cm^{-1} corresponds to the bending mode of water molecules[37]. Additionally, several absorption peaks below 800 cm^{-1} can be attributed to the stretching vibration patterns between the metal cation and oxygen atoms, such as Mg—O, Zn—O, and Al—O[36].

The results of the LDHs' thermal stability, measured by TGA, are presented in Figure 2- c. All samples exhibited a weight loss of up to 58% across four degradation stages. The TGA results indicate a step-by-step decomposition process, consisting of four stages. The first stage occurs between 50 °C and 150 °C, the second range between 150 °C and 255 °C, the third stage between 255 °C and 515 °C, and the fourth temperature range lies between 515 °C and 700 °C. In the first stage, water and absorbed gases are lost[38]. The weight loss during the second stage (150°C -255°C) is attributed to the loss of interlayer water molecules[39]. As mentioned earlier, the increase in the amount of Zn in LDHs formulations leads to a higher absorption of water between the layers due to the greater affinity of Zn towards water. Consequently, the weight loss values during this stage were observed to be 17.08%, 16.6%, and 15.8% for LDH-0.5R, LDH-R, and LDH-2R, respectively. In the third stage (255°C - 515°C), weight loss is associated with the decomposition of CO_3^{2-} anions, resulting in the release of CO_2 and water due to the dehydroxylation of OH groups[40]. As shown in Figure 2-d, with increased R ratios (which indicates a higher Mg content), the third stage shifts to a higher temperature, and the rate of mass loss increases. This shift to a higher temperature can be attributed to the greater thermal stability of the Mg-rich phases, which require more energy (higher temperature) to decompose. Consequently, the decomposition and subsequent weight loss are delayed.

The observation that LDH-0.5R exhibits a lower weight change in stage 3 (16.86%) is due to a greater loss of interlayer water molecules in stage 2. Conversely, with the increase in Mg content, the weight loss for LDH-R (19.54%) and LDH-2R (24.57%) increases in stage 3. This is because the higher Mg content leads to the formation of more thermally stable phases, resulting in greater weight loss at higher temperatures. The higher temperatures observed in the fourth stage (515 °C - 700 °C) can be attributed to the formation of metal oxides[41]. This stage entails the final decomposition and creation of stable metal oxide structures, which further contribute to the overall decrease in weight. Regarding the residual weight, it should be noted that despite the increased R ratio resulting in greater mass loss in stage 3, LDH-2R ultimately ends with a lower final weight. This can be explained by the overall extensive decomposition and loss of CO_3^{2-} and OH groups in the third stage, which more than compensates for the lesser weight loss observed in stage 2.

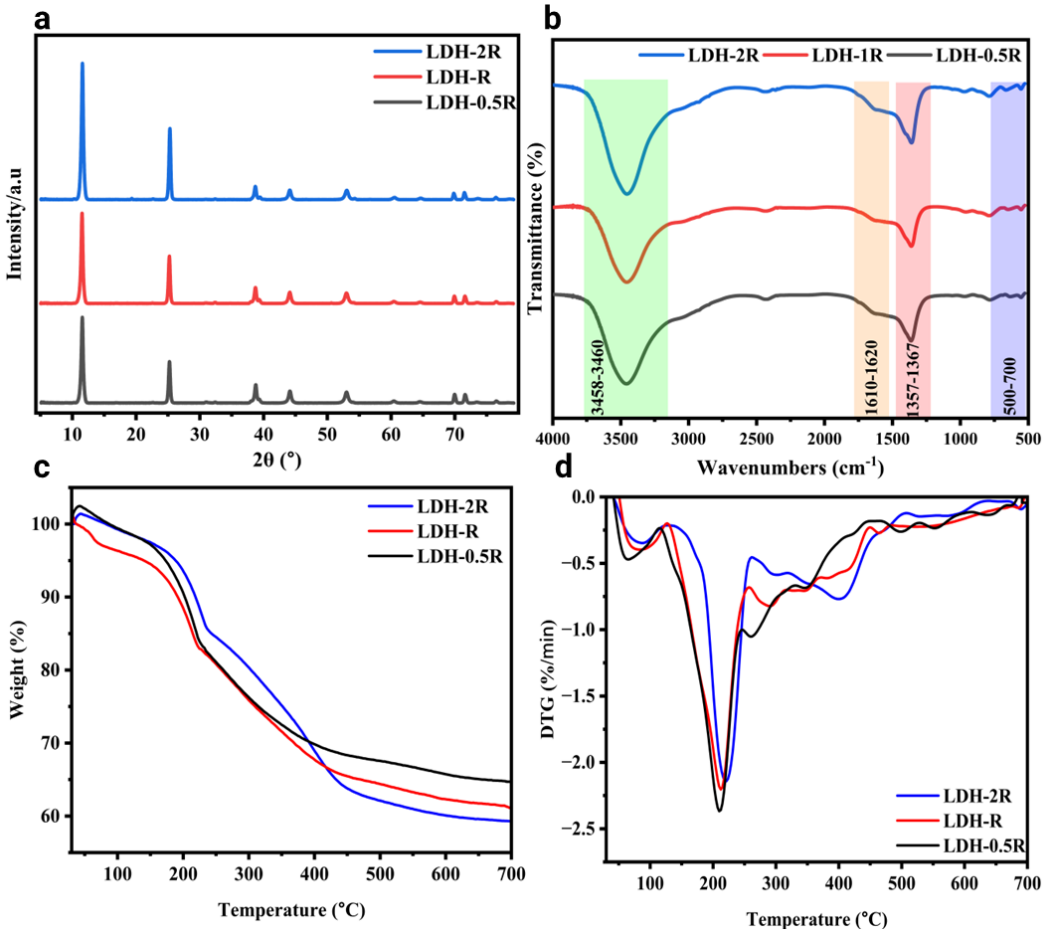

Figure 2 a) Powder X-ray diffraction patterns, b) FT-IR spectra, c) TGA, and d) DTG of LDH-0.5R, LDH-R and LDH-R2.

Table 2 shows the BET surface areas (δ_{BET}), total pore volumes (ν_p), and pore radius (R_p) for synthesized LDHs. The BET surface areas were obtained for LDH-2R, LDH-R, and LDH-0.5R samples 7.825 m^2g^{-1}, 7.752 m^2g^{-1}, and 7.732 m^2g^{-1}, respectively. Furthermore, the radius and volume of the pores decrease as the Mg/Zn ratio increases. This is evident from the greater X-ray diffraction intensity (Figure 2-a) of the LDH-2R compared to LDH-0.5R in the 003 phase, indicating a more packed and denser arrangement of crystal lattice structures. Additionally, the ICP analysis reveals that the ratios of Mg/Zn and (Mg+Zn)/Al are consistent across all samples, albeit with some minor deviation. Figure 3 displays the SEM images depicting the structure and morphology of the synthesized LDHs. The structure of LDH nanoparticles transforms from a lumpy structure to a hexagonal flake structure as the Mg/Zn molar ratio increases. The structural analysis confirms that the synthetic materials belong to the category of LDH materials, displaying various compositions within the metal host. In particular, the morphology of our LDHs in Figure 3 is well conssitent with the MgAlZn-LDH synthesized by Labuschagn [42] for thermal stabilizer application. Furthermore,

Zhou [43] demonstrated that the d_{003} basal spacing value for MgAlZn-CO_3 is 0.778 nm, which closely agrees with our findings.

Table 2 Structural Parameters and ICP-MS results of unmodified LDHs.

Sample ID (LDH)	δ_{BET} (m^2g^{-1})	v_p (cc g^{-1})	R_p (Å)	Atomic ratio (R^1)		M/Al^2	Formula
				Theoretical	Experimental		
0.5R	7.825	0.053	19.457	0.5	0.516	2.043	$[Mg_{1.20}Zn_{2.32}Al_{1.69}(OH)_{10.1}] (CO_3)_{5.07}$
R	7.752	0.053	19.232	1	1.006	2.087	$[Mg_{1.70}Zn_{1.69}Al_{1.66}(OH)_{10.1}] (CO_3)_{5.07}$
2R	7.732	0.051	19.194	2	2.041	2.146	$[Mg_{2.41}Zn_{1.18}Al_{1.67}(OH)_{10.1}] (CO_3)_{5.07}$

[1] Mg/Zn

[2] (Mg + Zn)/Al

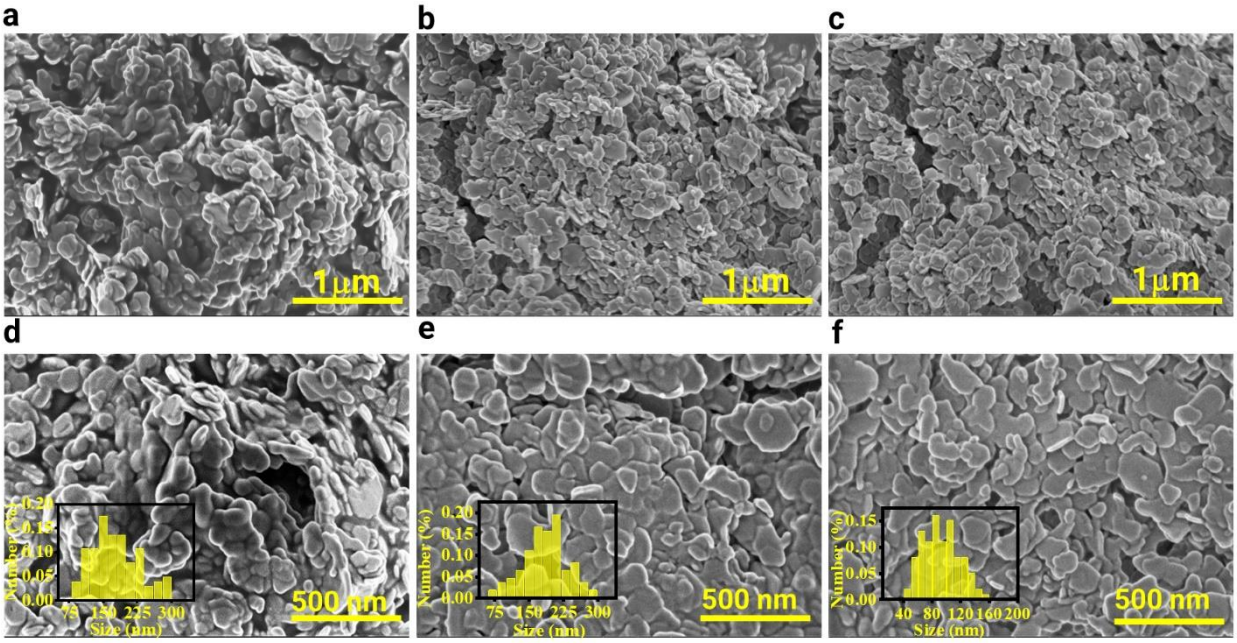

Figure 3 SEM images of a) LDH-0.5R, b) LDH-R, and c) LDH-2R (1µm, ×80 000). The bottom row shows the same materials at higher resolution: d) LDH-0.5R, e) LDH-R, and f) LDH-2R (500nm, ×150 000)

4.2. Impact of LDH on Thermal Properties of PVC Compounds

The FTIR spectra of PVC compounds containing the LDH materials are shown in Figure 4-a. In the CS samples, the peaks at 2957 cm^{-1} and 2925 cm^{-1} can be attributed to C-H stretching in CH-Cl and C-H stretching in CH_2, respectively[44, 45]. The peak at 1720 cm^{-1} corresponds to the C=O bond of DINP, while the peak at 1122 cm-1 corresponds to the C-O bond of DINP. Additionally, the peak at 1427 cm^{-1} signifies CH_2 bending, while the peak at 1354 cm^{-1} represents C-H bending in CH-Cl[46]. Furthermore, the peak at 1074 cm^{-1} corresponds to the C-C stretching of the PVC backbone[45], and the peak at 961 cm^{-1} signifies CH_2 bending. All the peaks at 830 cm^{-1}, 700 cm^{-1},

and 614 cm^{-1} can be assigned to C-Cl bonds[46]. The peaks at 1600 cm^{-1} and 1579 cm^{-1} are attributed to C=C bonds[44]. The peak at 1256 cm^{-1} represents the bending bond of C-H close to Cl[47]. With the introduction of LDHs to PVC compounds, the broad peak around 3420-3450 cm^{-1} indicates the presence of OH groups and interlayer H_2O of LDHs in the compounds. Additionally, the peaks at 583 cm^{-1} (Figure 4-b) and 611 cm^{-1} (Figure 4-c) are assigned to the metal-O stretching of LDHs[48].

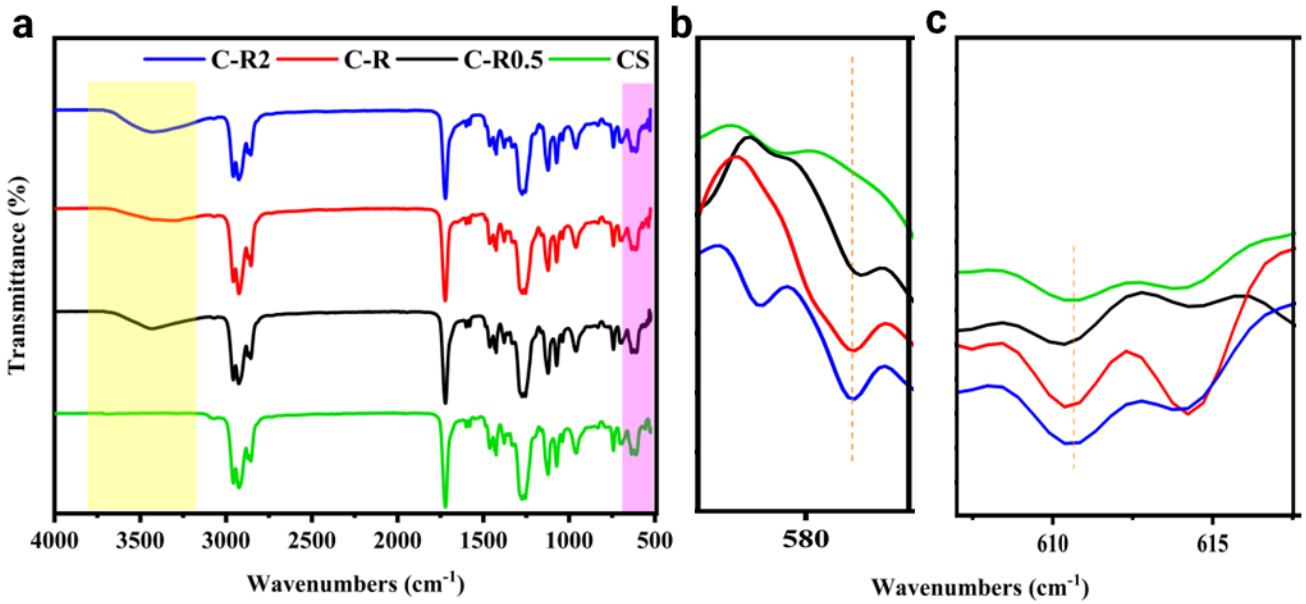

Figure 4 FT-IR spectra of a) unmodified PVC compounds and b-c) the enlarged view near metal-oxygen bands.

With the initiation of PVC degradation, HCl is released into the system. The starting time for this process can be determined using the Congo red test as a measure of STS[49] (Figure 5-a). The indicator paper of the CS compound changed from orange to red after 55 minutes, indicating the autocatalytic degradation of PVC and an increase in HCl concentration in the system. By incorporating LDHs into PVC compounds, the degradation time increased to 80, 87, and 96 minutes for the C-R0.5, C-R, and C-R2 samples, respectively. This corresponds to a 42% improvement in STS for the C-R2 sample compared to the CS, demonstrating the LDHs' ability to scavenge released HCl and inhibit PVC autocatalytic degradation. Labuschagne et al[38] reported with the incorporation of MgAlZn-LDH (Mg+Zn/Al=2) the STS increased from 25 to 98 minutes, which is closed to our results. In the dehydrochlorination test, PVC degradation was monitored using the water electroconductivity trend (Figure 5-b). In this method, the released HCl is carried by N_2 gas to deionized water, and the increasing rate of H^+ concentration indicates the rate of PVC degradation. Guo[50] et al. defined the onset time of degradation as the induction time (t_1), and the minimum point of electroconductivity as the stability time (t_2). For the C-R2 sample, the electroconductivity after 160 minutes was 4.35 mS/cm, while the corresponding times for the CS, C-0.5R, and C-R samples were

116, 130, and 145 minutes, respectively. This demonstrates that LDHs, particularly at higher Mg/Zn ratios, possess the highest capacity to regulate the release of HCl. The conclusion is consistent with the study by Wang et al.[51], which investigated the effect of metal compositions on HCl absorption in PVC compounds.

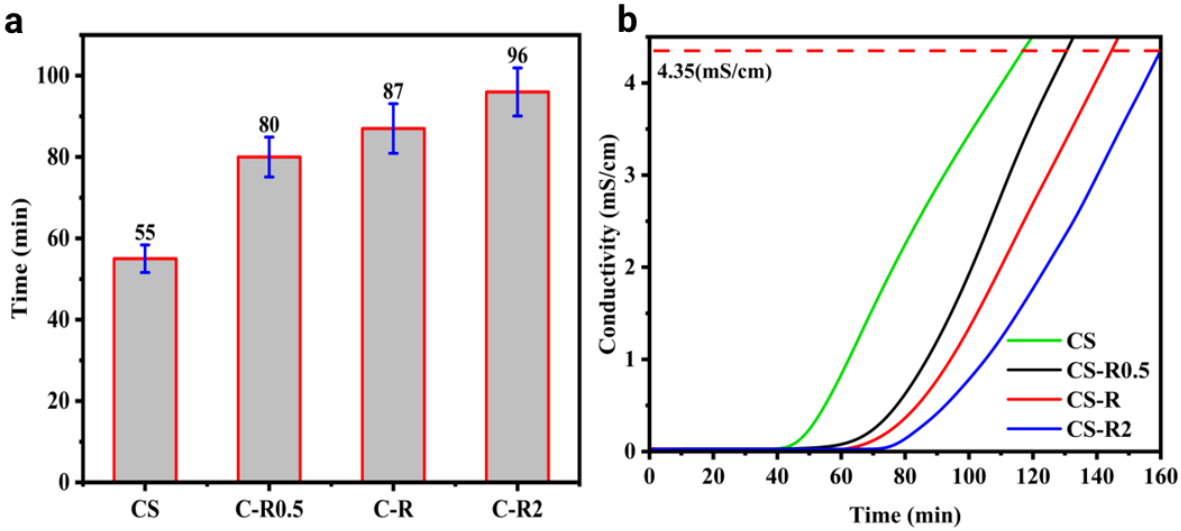

Figure 5 a) Static thermal stability (STS) at 180 ◦C, and b) HCl release curves for the PVC samples heated at 180 ◦C (Dehydrochlorination) of CS, C-0.5R, C-R, and C-R2 compounds.

The color changes of the samples, maintained at 180°C for 10 to 180 minutes, are depicted in Figure 6-a. Over time, all samples transitioned from yellow to brownish-yellow and eventually to black. The CS compound turned yellow after 20 minutes, and black spots appeared on the CS sheets after 70 minutes. The CS sample became black within 80 minutes, earlier than the degradation of all LDH-treated compounds. This suggests that the zipper autocatalytic dehydrochlorination process was more rapid in the CS sample than in LDH-treated samples[52]. During the early stages of testing, the C-0.5R compound demonstrated better color stability compared to C-R and C-R2 compounds. However, after 30 minutes, the C-0.5R sample rapidly changed color to brown. As discussed in the previous section, the Zn cation has a larger radius, and its electronegativity (1.65) exceeds that of Mg (1.31). These parameters have distinct effects on the thermal stability of PVC compounds over short and long durations[33]. In the short term, Zn's greater electronegativity influences the interactions between hydroxyl groups and host layers, while its larger radius weakens M-O bonds. These reactions facilitate HCl absorption by LDHs and prevent HCl migration within the system. However, in the long term, Zn can form $ZnCl_2$ groups during PVC degradation—a phenomenon known as zinc burn. This acts as a superior catalyst for the dehydrochlorination reaction, accelerating PVC degradation[53]. Figure 6-b,c illustrates the changes in ΔB and ΔE (in eq1) during PVC degradation. The ΔB value for CS-0.5R is initially lower than that of the C-R2 compound within the first 30 minutes. However, after 40

minutes, Δ*B* sharply increases and then decreases with a high slope. In contrast, the Δ*B* of the C-R2 compound increases more gradually, remaining nearly constant between 100 and 140 minutes before decreasing. This behavior highlights Mg's ability to enhance the long-term thermal stability of PVC compounds. Δ*E* follows a similar pattern. Initially, the C-0.5R sample exhibits better thermal stability than other LDH-treated samples. However, with increasing time, the C-0.5R sample experiences sharp increases in ΔE. Meanwhile, ΔE increases more moderately with Mg incorporation, and the ΔE value decreases when additional Mg is incorporated into the compounds.

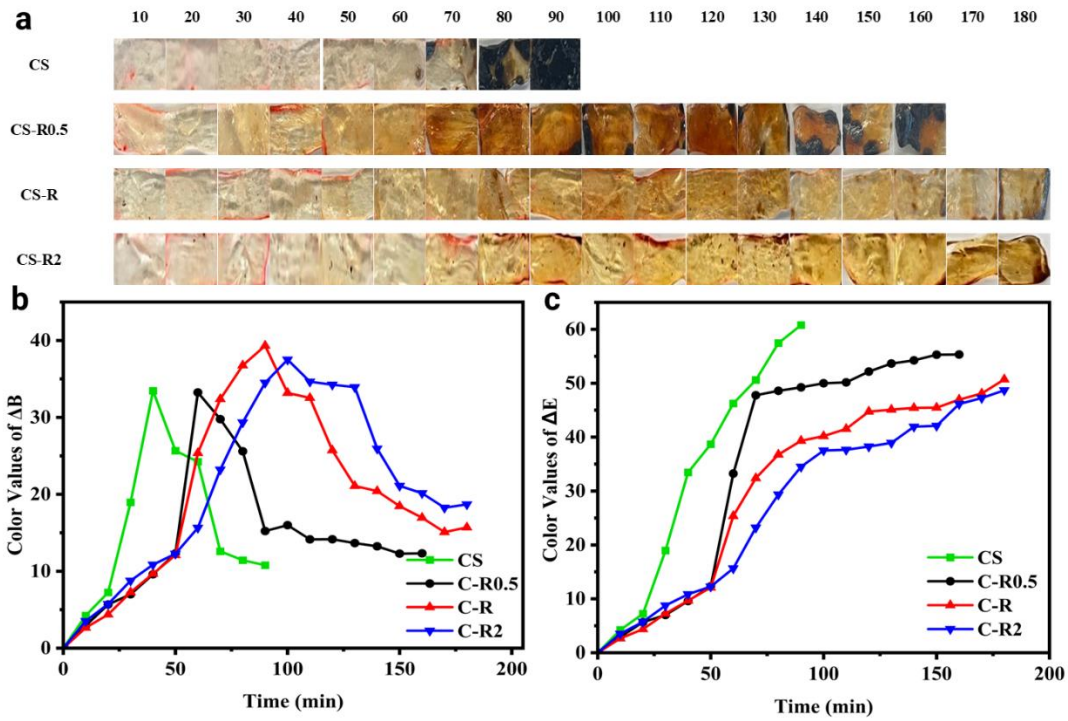

Figure 6 a) Changes in color profile of discoloration test for unmodified LDHs-PVC compounds at 180 °C from 10 to 180 minutes. Color change test results for a) ΔB and b) ΔE at 180 °C.

The thermal gravimetric analysis (TGA) and differential thermogravimetry (DTG) curves of PVC compounds in an N_2 atmosphere are presented in Figure 7-a and Figure 7-b, respectively. The curves reveal two distinct stages of thermal degradation in all the compounds. The first stage occurs within the temperature range of 250-400°C and is associated with dehydrochlorination. The second stage, which takes place between 400-550°C, is attributed to the degradation of polyene sequences and remaining polymer structures, as well as the formation of char[54]. Compared with the LDH-doped samples, the CS sample exhibits these stages at lower temperatures.

Detailed TGA data (in Table S-5) provide the assigned temperature for a 5% weight loss ($T_{5\%}$), which occurs after the T_{onset} (Figure 7-c), indicating that the CS sample has a higher or equivalent assigned temperature in comparison to the samples with LDHs. Furthermore, by incorporating LDHs

with a higher Mg content, the T_{max} shifted to a higher temperature (Figure 7-d), accompanied by a decrease in the intensity of weight loss.

LDHs belong to the suppressive class of PVC thermal stabilizers, meaning that they absorb or neutralize the HCl produced during PVC degradation[55]. The reaction mechanism between LDHs and HCl occurs in two stages. In the first stage, the HCl gas reacts with the available anions in the interlayer gallery, resulting in the exchange of chloride ions (Cl^-) and the formation of intercalated Cl between the layers. As the rate of PVC degradation increases and more HCl gas is released, the hydroxyl groups (OH^-) in LDHs neutralize the acidity of HCl by absorbing hydrogen ions (H^+), leading to the formation of water (H_2O) and chloride ions (Cl^-). Subsequently, the metal cations (M^{2+} and M^{3+}) within the LDH structures react with Cl^- to form metal chloride compounds, thus inhibiting the migration of HCl throughout the matrix[56]. Hence, owing to the substantial absorption capacity of LDHs, they can markedly enhance the thermal stability of PVC.

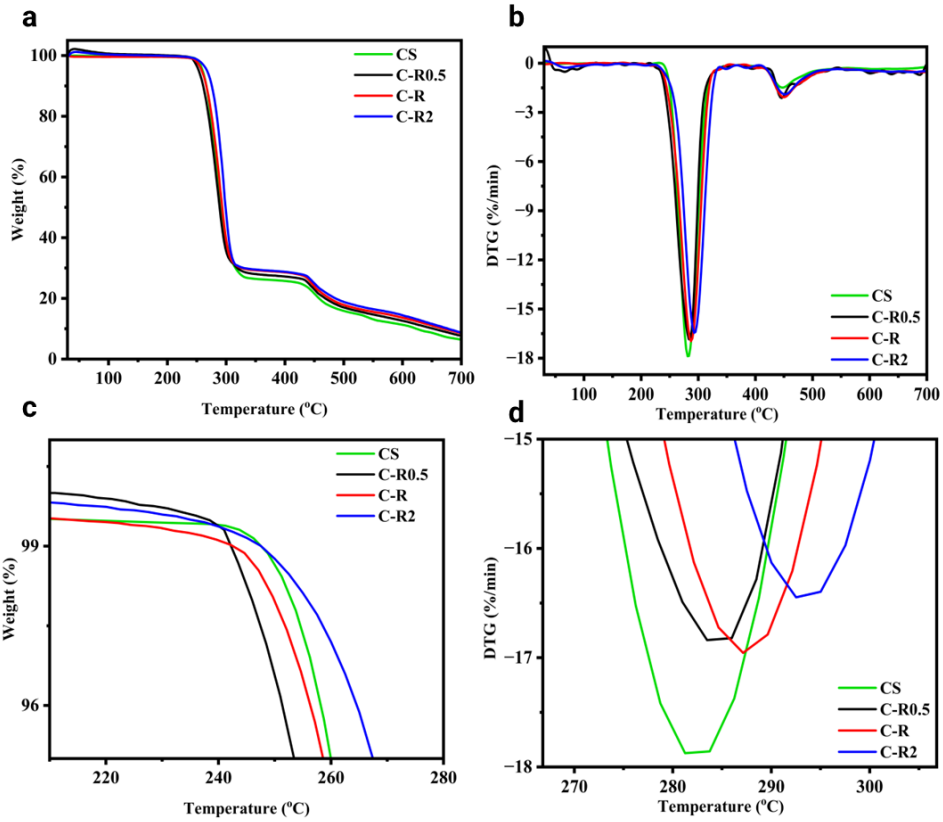

Figure 7 a) TGA, b) DTG, the enlarged view near c) T_{onset}, and d) DTG peak in stage I of CS, C-0.5R, C-R, and C-R2 compounds.

4.3. Surface Modification of LDH with Oleic Acid

When OA is introduced to LDH structures, it may either attach to the LDH surface through its carboxylic acid head or be placed between the layers[57]. These interactions directly impact the crystallinity of LDHs because of changes in the chemistry of the LDHs' surface and the interlayer distance[57]. Powder X-ray patterns showed (Figure 8 -a) distinct trends in the 2θ and FWHM values of LDHs modified with different amounts of OA.

The 2θ values for LDH-2R, LDH-2R-3OA, LDH-2R-6OA, and LDH-2R-9OA were relatively close, ranging from 11.58° to 11.61°. Additionally, the calculated basal space value (*c*) for these samples, as shown in Table 3, fell within the same range, indicating that, for these OA levels, OA groups are grafted onto the LDH surfaces, instead of being inserted between layers. As the amount of OA in the system further increased, it gradually entered the interlayer spaces, as demonstrated by the LDH-2R-12OA sample with a decrease in 2θ to 11.45° degrees and an increase in the c parameter to 2.180 nm.

Table 3 Lattice parameters of surface-modified LDHs compared with the unmodified case.

Sample ID (LDH-2R)	2θ (003) (°)	2θ (006) (°)	2θ (009) (°)	2θ (110) (°)	d_{003}	d_{003} intensity	FWHM$_{003}$	c (nm)	a (nm)	*D* (nm)
2R	11.588	25.3083	38.698	60.8283	0.763	22.32	0.407	2.163	0.2691	23.11
3OA	11.588	25.278	38.698	60.432	0.763	9.78	0.313	2.164	0.306	25.430
6OA	11.618	25.328	38.688	60.408	0.761	13.54	0.291	2.161	0.306	27.33
9OA	11.591	25.311	38.701	60.461	0.762	18.55	0.248	2.160	0.305	32.159
12OA	11.440	25.15	38.54	60.42	0.772	15.58	0.315	2.180	0.306	25.288

The FWHM value provides information about the size and strain of crystal structures [58]. Among the samples that underwent surface modification, LDH-2R-9OA demonstrated the smallest FWHM value of 0.248, as reported in Table 3. This suggests that, compared with both higher (12OA) or lower (3OA and 6OA) OA concentrations, a moderate concentration of OA can both enlarge the crystal size and reduce the distortion and defects in crystal structure (Figure 8 -b). The narrower peak in the spectrum indicates larger and more ordered crystals. Several factors can contribute to this phenomenon, including the surfactant properties of OA and its interaction mechanisms with LDH[59]. Each OA molecule possesses a hydrophilic carboxylic acid group and a long hydrophobic tail, which facilitate their adsorption onto LDH surfaces. As a result, the surface energy decreases, preventing the formation of defects and promoting improved crystallinity in LDH-2R-9OA. This leads to

favorable conditions for the growth of crystallites and the stabilization of LDH structures. In their early study of MgZnAl-LDHs, Xu et al. [60] showed that the presence of OA increased the FWHM value compared to the unmodified sample and reduced crystal agglomeration. Due to the lack of information on OA amount in that study, direct comparison with our results is not possible.

Furthermore, the intensity of the 003 peak in LDH-2R-9OA is lower than that of the LDH-2R sample, indicating initial disruption of the LDH structure and changes in nucleation and growth dynamics due to the influence of OA on LDH crystallization[61]. When OA is added to LDHs in lower concentrations, the intensity of the 003 peak decreases significantly, clearly demonstrating the effect of OA. However, with higher OA concentration, the intensity increases, particularly in the case of LDH-2R-9OA. Therefore, at lower concentrations, OA leads to an unstable situation for crystal reorganization and alignment. However, as the concentration of OA increases, the surface energy of LDHs decreases due to the surface-active effect of OA. This reduction in surface energy facilitates the nucleation and attachment of precursor ions to the surface, promoting the formation of stable nuclei and facilitating the nucleation process.

The FTIR spectra of OA reveal several characteristic peaks as shown in Figure 8 -c. The peak observed at 2860 cm^{-1} can be attributed to symmetric CH_2 stretching, while the peak at 2930 cm^{-1} corresponds to asymmetric CH_2 stretching modes[62]. The peak at 3007 cm^{-1} is due to the C–H mode of the C–H bond adjacent to the C=C bond[63]. Furthermore, the peak at 1710 cm^{-1} indicates the presence of C=O, which arises from the O–H stretch[64]. The LDHs that underwent surface modification exhibited peaks that were closely like those shown in Figure 2-b. Lei et al.[65] showed in the modification of LDH by fatty acid methyl esters that the hydroxyl (-OH) group on the surface of LDH and the carboxyl (-COOH) group on the fatty acid were chemically bonded by dehydration condensation. The vibrational peaks confirm this bonding observed at 2922 and 2852 cm^{-1}, which originate from methylene asymmetric and symmetric stretches. In addition, the peak at 940 cm^{-1} is –O–H out of the plane mode of the carboxylic acid [66], and the observed peak at 730 cm^{-1} is related to the out-of-plane bending vibrations of the C-H deformation bonds of the -CH=CH- group[67]. These features indicate the presence of long alkyl chains that are branched on the surface of the LDH-2R-XOA LDHs. Taken together, these results point to the successful modification of OA on the surface of LDH-2R-XOA.

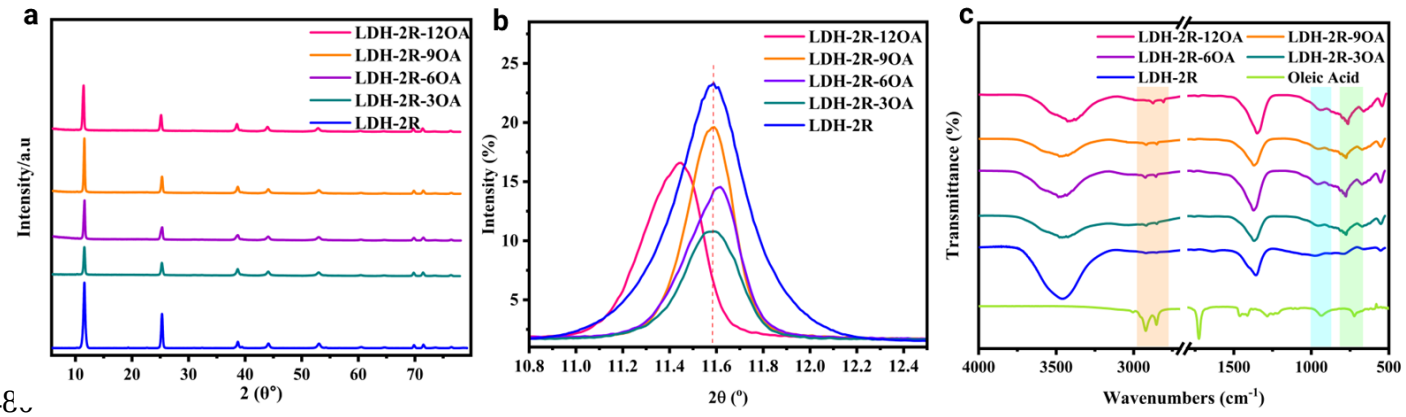

Figure 8 a) Powder X-ray diffraction patterns, b) Powder X-ray peaks of (003), and c) FT-IR spectra of LDH-2R (unmodified), LDH-2R surface modified with 3, 6, 9, and 12 OA.

The oxidation state and chemical compositions of these LDHs were investigated using X-ray photoelectron spectroscopy (XPS). Figure 9-a presents the XPS full spectra of both modified LDHs and LDH-2R, confirming the presence of oxygen (O), carbon (C), aluminum (Al), zinc (Zn), and magnesium (Mg) elements in the binding energy range of 0-1600 eV.

The high-resolution O 1s spectra in Figure 9-b reveals two peaks for LDH-2R samples and three peaks for surface-modified samples. The assigned binding energy for O 1s in LDH-2R is 531.7 eV as reported in [68] before. However, after the surface modification process, the binding energy of the O 1s peak in LDH-2R-3OA, LDH-2R-6OA, LDH-2R-9OA, and LDH-2R-12OA changes to 531.49 eV, 531.59 eV, 531.53 eV, and 531.74 eV, respectively. This indicates a significant effect of octadecyl chains on the LDHs' surface, where the C=O structures with a binding energy of 530.8 eV for LDH-2R-3OA demonstrate the interaction between the carboxylic group of OA and the -OH group on the surface of LDHs[60]. The peak area of H_2O in LDH-2R is 73.6%, while the H_2O peak area in LDH-2R-3OA, LDH-2R-6OA, LDH-2R-9OA, and LDH-2R-12OA is 41.81%, 32.69%, 34.43%, and 34.27%, respectively. These changes indicate alterations in the surface chemistry of the modified samples. Additionally, the lattice-oxide (M-O) group in LDH-2R is assigned a binding energy of 529.9 eV, which decreases by 0.49 eV after surface modification, resulting in a decrease in surface energy[68]. This decrease in surface energy contributes to the chemical stability of LDHs and improves their thermal decomposition at higher temperatures[60]. The C 1s XPS spectra as demonstrated in Figure 9-c show three peaks for modified and unmodified LDHs. The C–C bonds are observed around 284.45-284.5 eV, C–OH bonds at 285.3-285.7 eV, and CO_3^{2-} groups at 289.4-289.5 eV. The intensity of C-C bonds increases from 3600 counts cp for LDH-2R to 4600 cp for LDH-2R-9OA, indicating the successful branching of octadecyl chains on the LDH surface, thus creating a hydrophobic environment around the LDH crystals[41]. Furthermore, with an increase in OA content,

the CO_3^{2-} group decreases, especially in the LDH-2R-12OA sample, suggesting that the OA chains enter the LDH interlayer and increase the distance between layers. The spectra of high-resolution Mg 1S (1303.5 eV), Al 2p (74.4 eV), Zn $2p_{3/2}$ (1021.8 eV) and Zn $2p_{1/2}$ (1044.8 eV) which shown in Figure S-4, did not show significant changes in binding energy and peak intensity, indicating that the LDHs matrix remains unaffected by OA and that the metal sites are stable[69, 70].

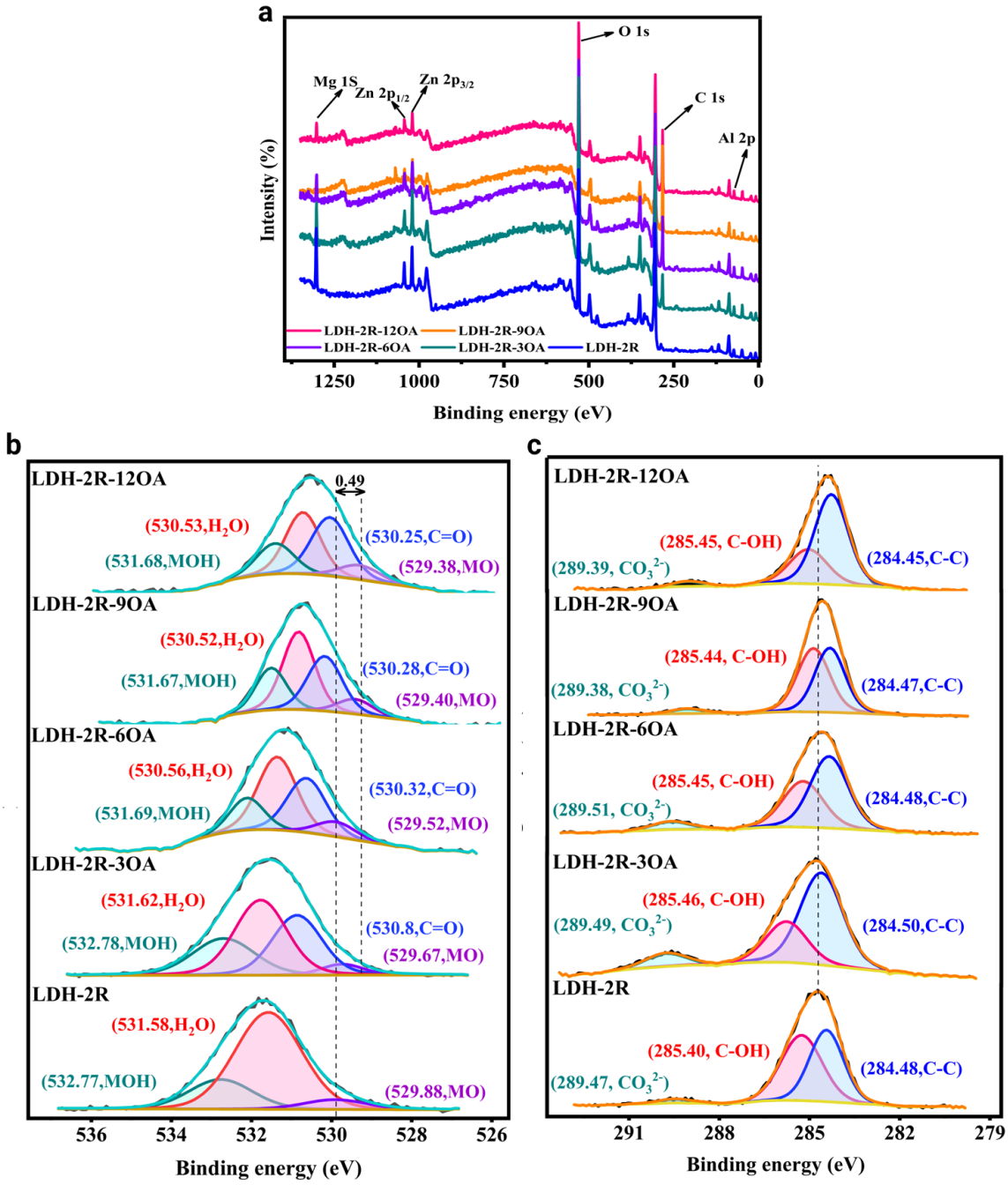

Figure 9 a) XPS spectra of the original and surface-modified LDHs, XPS spectra for b) O 1s, and c) C 1s.

To quantify the amount of modification and the impact of surface modification on the thermal stability of LDHs, TGA was conducted. As depicted in Figure 10-a, the modified LDHs exhibit the same four stages of thermal decomposition as the unmodified samples. In the temperature range of 50-120°C, the changes in sample weight correspond to the desorption of physisorbed molecules[71]. However, comparing LDH-2R with that of LDH-2R-12OA, the rate of mass loss decreases from 3.22% to 1.69%. This reduction in weight loss suggests that the modification reduces the release of water molecules, indicating that the modified samples are less hydrophilic and more hydrophobic. The incorporation of OA in LDH-2R-12OA likely enhances the hydrophobicity of the samples by making the surface less accessible to water, thereby reducing the amount of water retained and released during thermal decomposition. In addition, with the increase in the OA content, the second stage (120-225°C) shifted to higher temperatures (Figure 10-b) and the rate of weight loss decreased as well. The cause of weight loss can be attributed to the presence of interlayer water molecules and the initial dehydroxylation of OH groups in the second stage. As shown in Figure 10-c, the weight losses at temperatures of 220°C, 232°C, 235°C, 237°C, and 240°C are 15.8% for LDH-2R, 14.5% for LDH-2R-3OA, 14.1% for LDH-2R-6OA, 13.8% for LDH-2R-9OA, and 13.3% for LDH-2R-12OA, respectively. The main event occurs in the third stage (255-504°C), involving the decomposition of interlayer anions and OA, as well as further dehydroxylation, which is more complex[72]. With an increase in OA content, the thermal degradation of this stage shifts to higher temperatures, indicating that OA improves the thermal stability of LDH samples. In a series of studies on LDHs modified with fatty acids, Xu et al.[72, 73] demonstrated that in an inert environment, the degradation of organic content occurs through several processes, such as dehydrogenation, thermal cracking, and graphitization. They also suggested that the shift in decomposition to higher temperatures is due to the formation of more hydrocarbons instead of CO_2, thereby enhancing the thermal stability of OA-modified LDH samples. Furthermore, in this stage, the modified samples experience more weight loss, indicating the thermal decomposition of OA. These results are consistent with Zhang et al.'s [60] findings on LDHs modified by OA. Lastly, in the fourth stage (504-700°C), the weight loss varies, with samples containing higher OA content showing more significant weight losses due to the final decomposition of OA residues and the transformation into layered double oxide (LDO)[71].

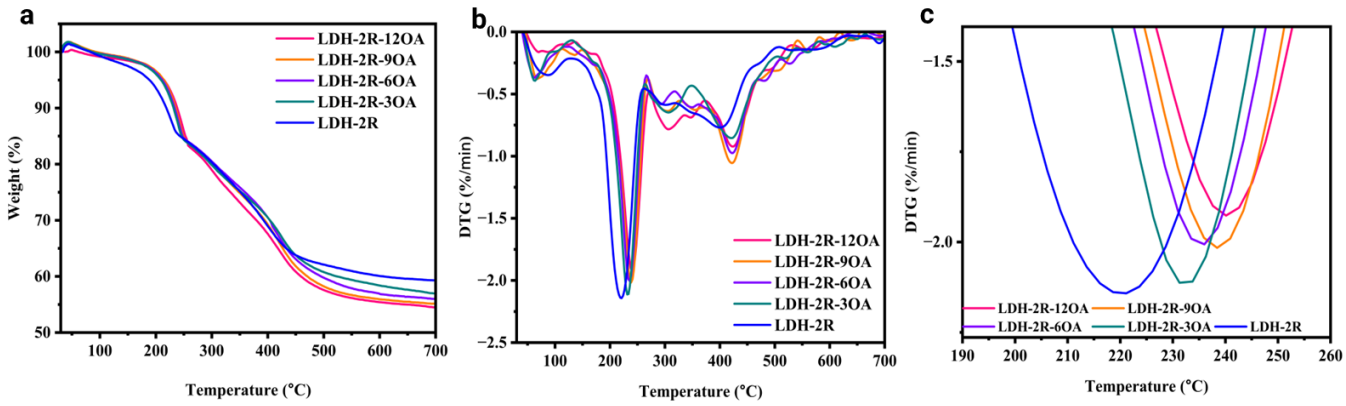

Figure 10 a) TGA, b) DTG, and c) DTG peaks (enlarged near stage II) of LDH-2R (unmodified), LDH-2R surface modified with 3, 6, 9, and 12 OA.

The textural parameters and the experimental atomic ratios obtained through ICP analysis are presented in Table 4. As the OA to LDH ratio increases from 3 to 12, the specific surface area exhibited a gradual increase from 8.025 to 8.852 m^2/g. Additionally, the pore size increased significantly from 15.3 to 19.2 with the increase in the amount of OA, which suggests that grafting oleic acid leads to the widening of existing pores or the formation of larger pore structures within the material.

The amount of grafting was this study is calculated by measuring the weight loss of the LDHs-OA samples, in accordance with the Tong[74] method for surface-grafted LDH. The grafting amount was determined using TGA weight loss analysis. After the thermogravimetric process, the remaining substances were identified as MgZnAl mixed metal oxides (MMO), with the formula $Mg_4Zn_2Al_3O_{10}$ based on the atomic molar ratio. These MMOs were decomposed from MgZnAl-CO_3-LDHs. By considering the molecular formula of LDHs, $Mg_4Zn_2Al_3(OH)_{21}CO_3$, the amounts of grafted polymers were calculated using the following equations:

$$\omega_{OA} = 1 - \omega_{MMO}\left(\frac{M_{LDH}}{M_{MMO}}\right)$$

M_{LDH} and M_{MMO} represent the relative molecular mass of MgZnAl-CO_3-LDH and the remaining MgZnAl-MMO after thermogravimetric tests respectively. The grafted polymers (ω_{OA}) were then quantified based on the residual weight ratio of MgZnAl-MMO (ω_{MMO}). The results showed that the amounts of OA grafted on the surface of LDH-2R-3OA, LDH-2R-6OA, LDH-2R-9OA, and LDH-2R-12OA were 49%, 51%, 59%, and 58% respectively. As evident from the data, LDH-2R-9OA and LDH-2R-12OA display comparable quantities of grafted OA. It is thus inferred that a portion of extra OA added in LDH-2R-12OA is inserted between the layers based on the X-ray results in Table 3. As

the XPS results showed grafting process of OA onto LDHs induces a modification in their surface chemistry, resulting in a transition from hydrophilic to hydrophobic properties. Hydroxyl groups present between the layers act as a driving force that facilitates the migration of OAs from the synthesis medium to the interlayer space. Figure S-5 depicts the reaction between OA and MgAl-LDH illustrating the interaction between OA and LDHs. Moreover, the morphology of surface-modified LDHs presented in Figure 11 indicates that with an increase in OA, the surface of the LDHs becomes rougher.

Table 4 Textural Parameters and ICP-MS results of surface modified LDHs.

Sample ID	δ_{BET} (m^2g^{-1})	v_p (cc g^{-1})	R_p (Å)	Atomic ratio (R^1)		M/Al[2]	Formula
				Theoretical	Experimental		
2R-3OA	8.025	0.039	15.326	2	2.037	2.140	$[Mg_{2.42}Zn_{1.19}Al_{1.69}(OH)_{10.1}](CO_3)_{5.07}(CH_3C_{16}H_{30}CO)_{3.3}$
2R-6OA	8.257	0.048	15.278	2	2.063	2.088	$[Mg_{2.38}Zn_{1.56}Al_{1.69}(OH)_{10.1}](CO_3)_{5.07}(CH_3C_{16}H_{30}CO)_{6.3}$
2R-9OA	8.556	0.035	19.250	2	2.028	1.99	$[Mg_{2.39}Zn_{1.18}Al_{1.79}(OH)_{10.1}](CO_3)_{5.07}(CH_3C_{16}H_{30}CO)_{9.01}$
2R-12OA	8.852	0.045	19.182	2	2.033	1.99	$[Mg_{2.39}Zn_{1.19}Al_{1.79}(OH)_{10.1}](CO_3)_{5.07}(CH_3C_{16}H_{30}CO)_{11.3}$

[1] Mg/Zn

[2] Mg+Zn/Al

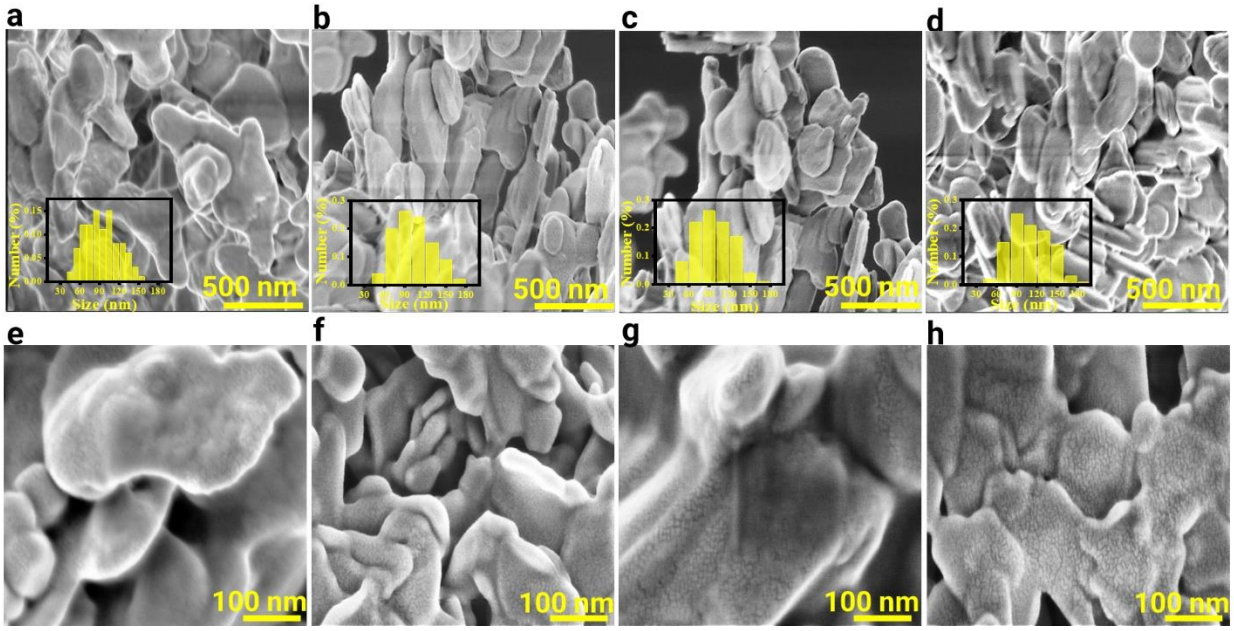

Figure 11 SEM images of a) LDH-2R-3OA, b) LDH-2R-6OA, c) LDH-2R-9OA, and d) LDH-2R-12OA (500 nm, ×150 000 000). The bottom row shows the same materials at higher resolution: e) LDH-2R-3OA, f) LDH-2R-6OA, g) LDH-2R-9OA, and h) LDH-2R-12OA (100 nm, ×500 000 000).

4.4.Thermal Stability Enhancement in LDH/OA-PVC Compounds

The modified LDH compounds were prepared using the same process as the unmodified compounds, and the detailed formulations are presented in Table S-6. As shown in Figure S-6, the surface-modified LDHs did not affect the transparency of PVC sheets.

The STS results for the modified compounds and C-R2 are presented in Figure 12-a. After the incorporation of OA, the STS duration increased from 96 minutes for C-R2 to 112, 121, 136, and 128 minutes for MC-3OA, MC-6OA, MC-9OA, and MC-12OA, respectively. It is worth noting that the STS duration for MC-9OA improved more than two times compared with the CS (i.e., no LDH). Compared with unmodified LDH (C-R2), the improvement is also over 40%, which is higher than similar approaches explored in the literature. The closest example for comparison is a Ca/Al binary LDH studied by Yang et al. [75] here they showed that modification by sodium stearate increased the STS duration from 90 mins (similar to our unmodified case) to 110 mins.

These findings demonstrate the direct impact of the organo-modification process of LDH nanoparticles on the thermal stability of PVC. Furthermore, the dehydrochlorination test (Figure 12-b) revealed that the compound with an OA/LDH ratio of 9 mmol exhibited a lower rate of HCl release. As the quantity of OA used as a surface modifier increased, the induction time also increased to 80 and 88 minutes for MC-9OA and MC-12OA, respectively. Moreover, at a conductivity of 2.97 mS/cm, the stability time for MC-9OA was 84 minutes, while for the C-R2 sample, it was 62 minutes.

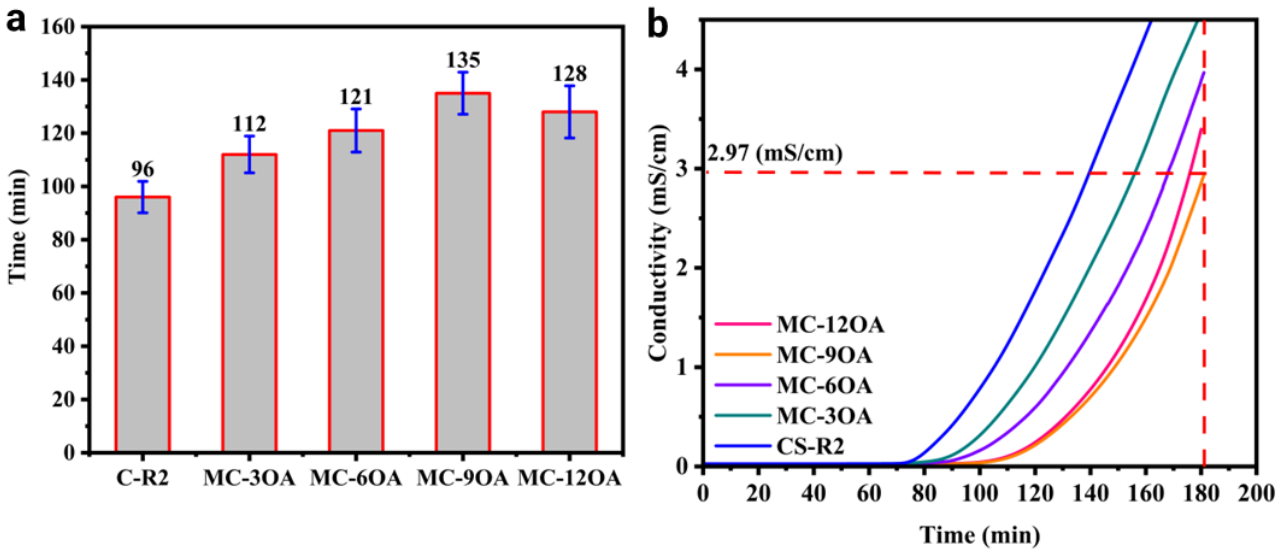

Figure 12 a) Static thermal stability (STS) at 180 °C, b) HCl release curves for the PVC samples heated at 180 °C (Dehydrochlorination)

The discoloration tests yielded significant findings regarding the color change behavior of the modified samples, as depicted in Figure 13-a. Initially, all the modified samples exhibited a consistent color for the first 50 minutes of the test at 180°C, except for MC-12OA. During the second stage of

color change, the modified samples gradually transitioned to yellow for 100 minutes, after which a yellowish-orange shade emerged. As time progressed, the color shifted to a light orangish brown, and none of the modified samples displayed black areas on the surface of the sheets. In the presence of OA, the color profile of the compounds underwent two distinct changes. In the case of the unmodified samples (Figure 6-a), black spots appeared and expanded as time elapsed, whereas the modified samples did not exhibit these spots. This observation suggests that OA enhances the interactions between the LDHs and PVC, resulting in homogeneous and stable compounds.

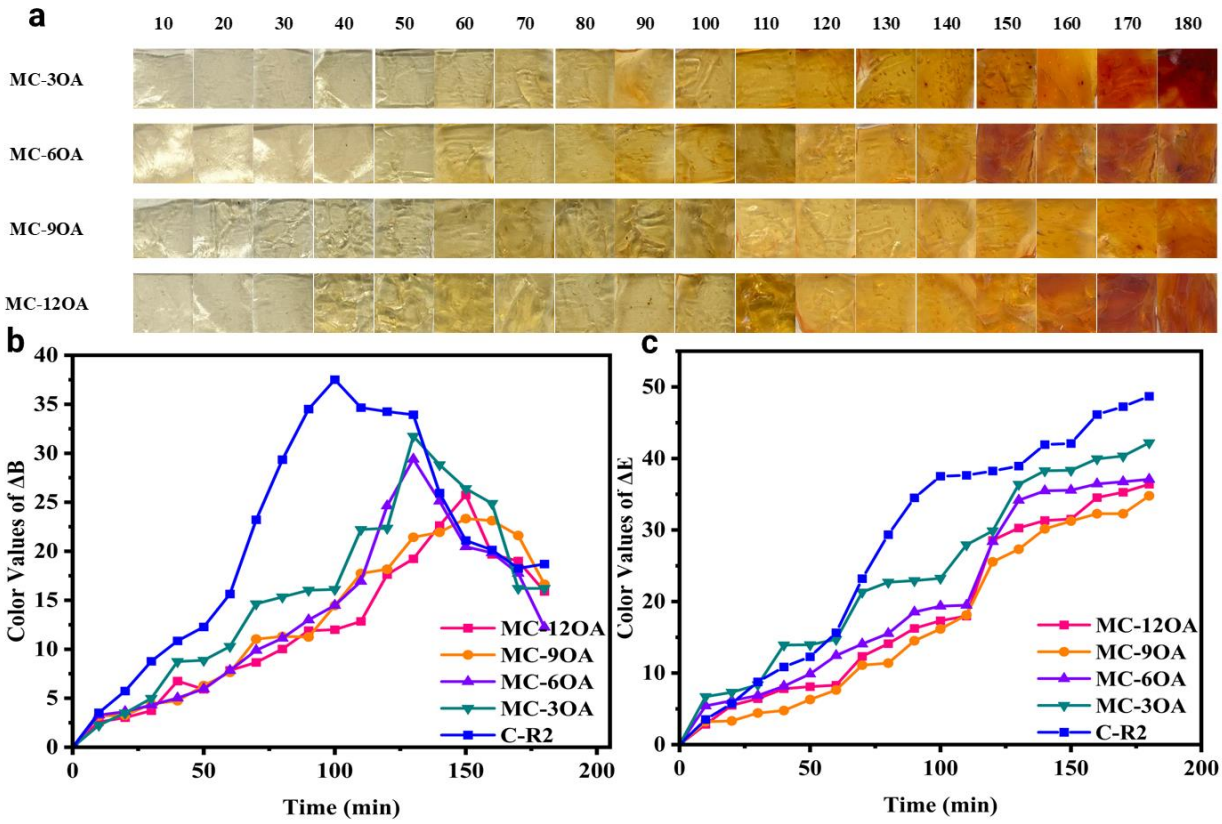

Figure 13, a) Color changes profile of discoloration test, discoloration test results for b) ΔB and c) ΔE at 180 ˚C of MC-3OA, MC-6OA, MC-9OA, and MC-12OA modified compounds.

The SEM images obtained from the cross-section of the samples confirm that the addition of OA improves the compatibility between PVC and LDHs. As depicted in Figure 14-a, there are noticeable gaps observed between the LDHs and PVC in the C-R2 samples. However, after the surface modification process, these gaps were eliminated (Figure 14-b) and enhanced interaction between LDHs and PVC was observed at the interface. In the unmodified case after thermal aging (Figure 14-c), the agglomerated LDHs were even segregated from the matrix. Conversely, the modified compounds exhibited a stable surface even after thermal aging, as shown in Figure 14-d. The SEM images of the modified compounds displayed consistent and unidirectional stripes. Similar morphological changes were observed in other modified thermal stabilizers. For example, Li et al.

[76, 77] studied zinc-based thermal stabilizers modified by tung oil fatty acids [77] and dicarboxylic acids [76] and attributed the observed morphological changes to the fatty acids' ability to improve the compatibility between the polymer and additives. This compatibilization effect facilitated the formation of stable structures, even under thermal aging conditions. Another study [78] investigated the modification of zinc metal alkoxide with di-mannitol adipate as a thermal stabilizer, which resulted in a plasticizing effect on PVC. The roles of compatibilization and plasticization effects of OA grafting on the materials morphology and properties will be a subject of our further investigation.

Additionally, in the unmodified samples, the color profile in Figure 6-a transitioned directly from yellow to brown, indicating a rapid progression of PVC degradation. In contrast, the modified compounds exhibited a color shift from yellow to orange and then to brown, suggesting a more gradual degradation process. This slower transition implies that OA effectively suppresses the auto-catalytic effect of PVC degradation, slowing down the overall degradation process. The changes in sheet color are represented by ΔB and ΔE (eq1) in Figure 13-c and d, respectively. The disparity in ΔB values between the modified and unmodified compounds is evident in Figure 13-c. The incorporation of OA leads to a decrease in ΔB_{max} and a shift towards higher temperatures. Furthermore, the rate of ΔB exhibits a slight increase with a higher amount of surface modifier in the compounds. For instance, in MC-9OA, within the 130–170-minute range, ΔB demonstrates a gradual transition from orange to brown, as depicted in Figure 13-a. Moreover, the treated samples exhibit lower ΔE values, and these values moderately increase with time.

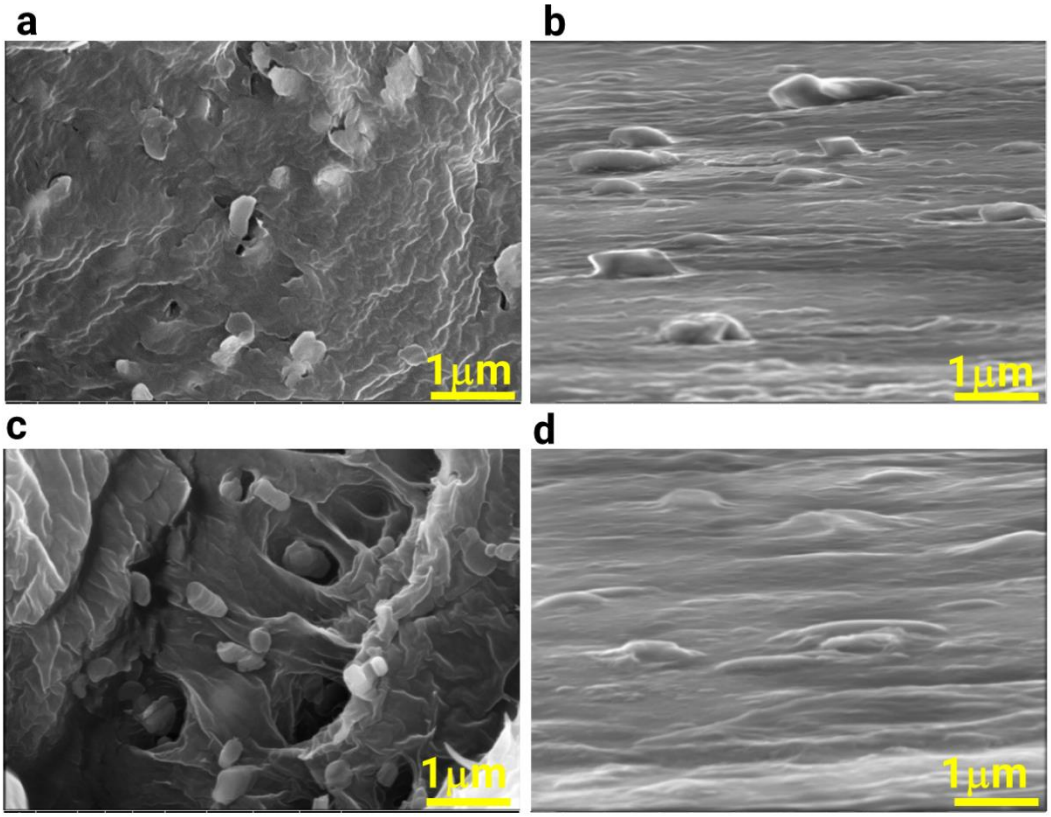

Figure 14 SEM image from cross-sections of a, c) C-R2 and b, d) MC-9OA. a, b) are before thermal aging, and c, d) after 180 minutes of thermal aging.

To investigate the thermal stability of the treated compounds, TGA and DTG curves were obtained for all samples, as illustrated in Figure 15-a and Figure 15-b, respectively. As shown in Figure 15-a, the modified compounds exhibited the same stages as the unmodified samples. In stage I, with the addition of LDH-OA to PVC compounds, the T_{onset} decreased with a slight difference compared to the C-R2 sample, as highlighted in Figure 15-c. The slight decrease in T_{onset} is attributed to the presence of small molecules and physically adsorbed OA molecules, rather than chemical bonding[20]. Consequently, the $T_{5\%}$ after T_{onset} is either lower or equal to that of the C-R2 compound, as reported in Table 5. As the temperature increases and the HCl absorption mechanism is activated by LDHs, C-From R2 to MC-9OA, $T_{25\%}$ increased from 287°C to 295°C. Moreover, with the incorporation of OA, T_{1Max} shifted to a higher temperature. The T_{1max} values for MC-6OA, MC-9OA, and MC-12OA are 296°C, 310°C, and 309°C, respectively. All these values exceed the T_{1max} of the C-R2 sample (292°C), except for MC-3OA.

It is worth noting that the intensity of the DTG peak decreases as the OA content in the compounds increases, as shown in Figure 15-b and d. This phenomenon indicates the effect of the surface modification process on enhancing the thermal stability of PVC compounds. Several key factors contribute to the enhancement of PVC compounds by OA. As observed in SEM results, the

introduction of surface-modified LDHs with fatty acid to PVC improves the compatibility between the nanoparticles and the matrix[21]. Furthermore, surface modification with OA improves the dispersion of hydrophobic LDHs in PVC and reduces the nanoparticles' agglomeration which could act as thermal degradation sites[21]. Additionally, in the presence of OA, LDHs exhibit a more uniform distribution, resulting in more consistent and stable compounds. EDS results confirm this assumption, As shown in Figure S-7 the EDS results showed a uniform distribution for modified LDHs with high dispersity in the matrix while the unmodified samples show the LDH's agglomerations with weaker dispersity than the modified sample (Figure S-8).

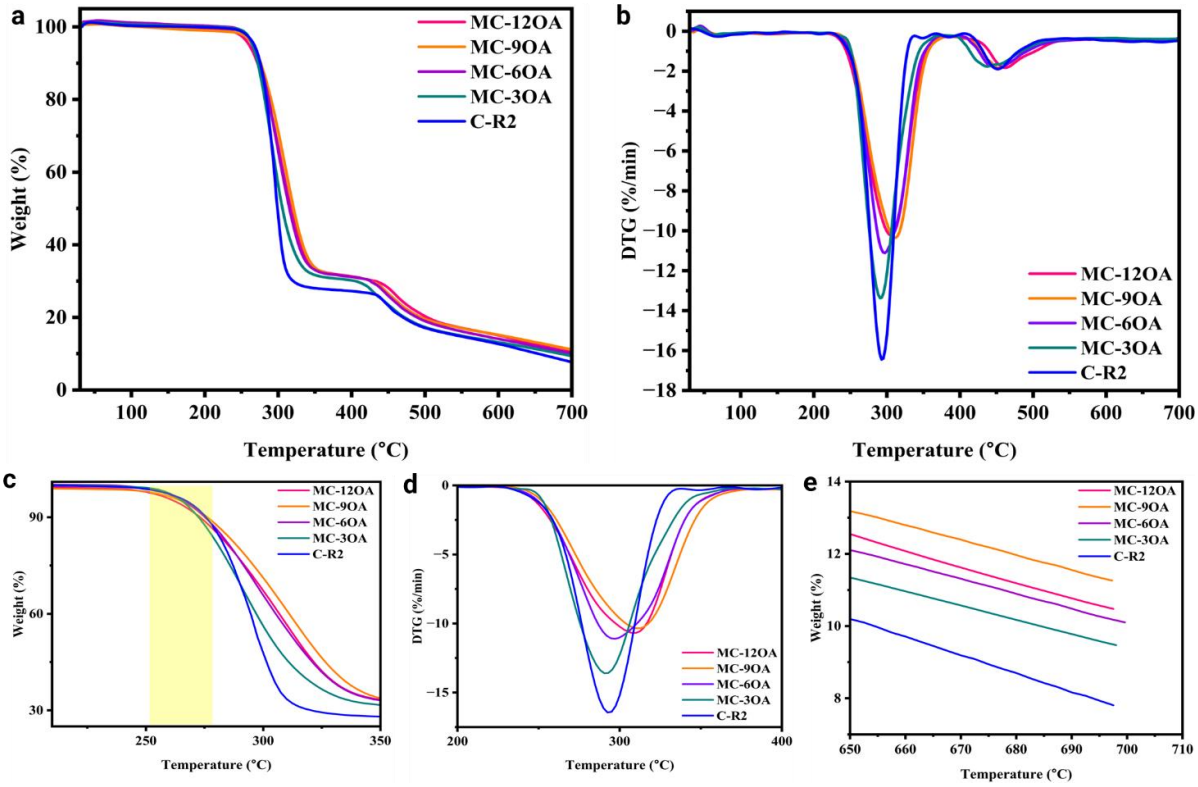

Figure 15 a) TGA, b) DTG, c) enlargement of TGA near stage I, d) enlargement of DTG near T_{max} of Stage I, and e) residual weight (%) in TGA of MC-3OA, MC-6OA, MC-9OA, and MC-12OA modified compounds.

Furthermore, the hydrophobic effect of OA acts as a barrier against destructive polar factors (such as $ZnCl_2$, Cl^-, and oxygen), thereby slowing down their migration to the matrix and resulting in reduced weight loss and color change rate.

679 **Table 5 TGA results of surface-modified LDHs-PVC compounds.**

Sample	$T_{5\%}$	$T_{25\%}$	$T_{50\%}$	$T_{80\%}$	T_{1Max} (°C)	T_{2Max} (°C)	W_R(%)
C-R2	265	287	299	470	292	452	8.65
MC-3OA	266	286	305	472	292	438	9.46
MC-6OA	265	290	315	489	296	452	10.12
MC-9OA	265	295	320	495	310	452	11.25
MC-12OA	262	292	317	497	309	455	10.48

680

681 The weight residue (WR%) values from the TGA results indicate the amount of material remaining
682 after the thermal degradation process. As shown in Figure 15-e, the WR% is 8.65% for the unmodified
683 sample (C-R2), whereas the OA-modified samples exhibit higher WR% values, which increases from
684 MC-3OA (9.46%), to MC-6OA (10.12%), and to MC-9OA (11.25%), with a slight decrease in MC-
685 12OA (10.48%). The increase in WR% with the addition of OA suggests that the modified LDHs
686 enhance the formation of char during degradation. The char can act as a protective barrier which slows
687 down the decomposition of the remaining material. The slight decrease in WR% for MC-12OA
688 indicates that is has passed the optimal level of OA content for maximum thermal stability. Overall,
689 the presence of OA in the LDH samples contributes to a higher residual weight, demonstrating
690 improved thermal resistance and char formation during the thermal degradation process.

691 **4.5.Discussions: Degradation Mechanisms and Kinetics**

692 Thus far, we have investigated the effects of LDHs with varying compositions and studied the
693 impact of organic surface treatment on both LDHs and PVC compounds. Based on our findings, we
694 considered C-R2 as the finest unmodified compound, while MC-9OA was the best-modified
695 compound for further in-depth study.

696 **4.5.1. Polyene index and Polyene length**

697 To investigate the correlation between the rate of thermal degradation and surface modification of
698 LDHs following the discoloration test, three samples were selected for further analysis: one after 10
699 minutes, 90 minutes, and 180 minutes that showed in Figure 13-a. These samples were selected from
700 the C-R2 and MC-9OA compounds. The samples are labeled with the aging time at the end: e.g., C-
701 R2-90 is the sample with unmodified (R = 2) LDH after 90 minutes.

702 Raman spectroscopy was employed to examine metal chloride structures within the range of 130-
703 330 cm^{-1}, which has been widely used by researchers to investigate diverse complex structures[79].
704 As depicted in Figure 16-a, the compounds before thermal treatment exhibited only background noise
705 within the chosen range. However, after 10 minutes, two broad peaks at 220 cm^{-1} [80]and 250 cm^{-1}

706 [81]emerged, both of which can be attributed to $ZnCl_2$. As previously mentioned, zinc possesses
707 greater electronegativity, a larger atomic radius, and a higher affinity for absorbing HCl than Mg.
708 Furthermore, due to the utilization of a Ca/Zn thermal stabilizer in the compound formulation, zinc
709 exhibits a higher level of overall incorporation into the compound compared with other elements.
710 Hence, the earliest appearance of the $ZnCl_2$ peak is not unexpected.

711

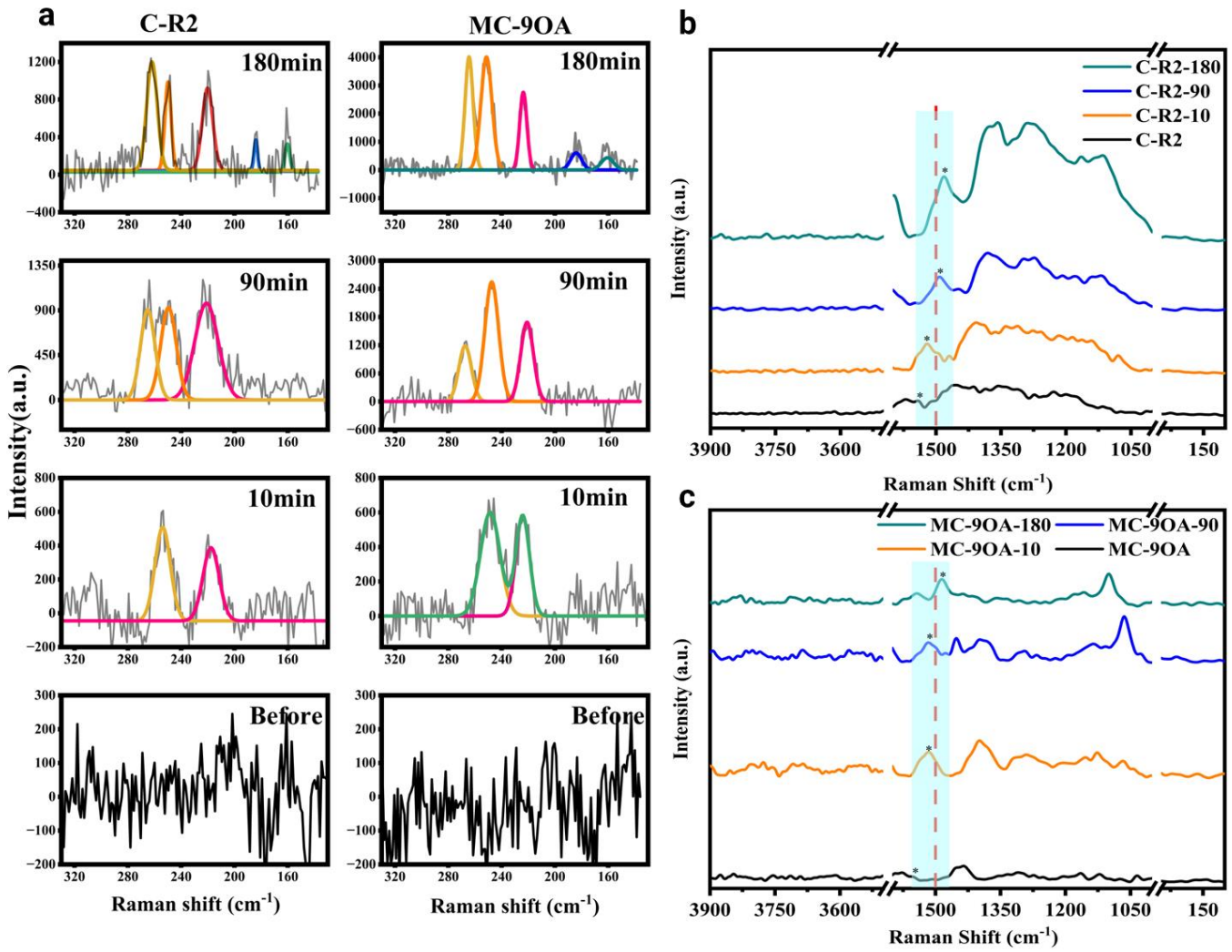

712

713 **Figure 16 a) Multiple-peak fitting of Raman spectroscopy of C-R2 and MC-9OA compounds at 180 °C after**
714 **10, 90, and 180 min, Change of polyene length for b) C-R2, and c) MC-9OA compounds with time (10, 90, 180)**
715 **at 180 °C.**

716 After 90 minutes, a new peak emerged at 265-267 cm^{-1} in both samples, signifying the presence of
717 $MgCl_2$ [82]which overlapped with $ZnCl_2$. The FWHM of C-R2 was found to be lower than that of
718 MC-9OA in both the 220 and 250 cm^{-1} peaks, while the intensity and area of MC-9OA were observed
719 to be higher than those of the C-R2 compounds. This trend was also observed for $MgCl_2$ around 260

720 cm^{-1} (Table S-7). In the initial stages of degradation, the lower FWHM of the unmodified compounds
721 (C-R2) suggests more organized structures and enhanced interactions in comparison to the MC-9OA
722 sample with PVC. The results of the dehydrochlorination test (Figure 12-b) illustrate that HCl is
723 released at a higher rate in C-R2 than in MC-9OA. Therefore, the lower FWHM of the C-R2 case is
724 a result of higher initial HCl concentration. As degradation progresses and additional HCl is released,
725 the intensity and area under the peak for MC-9OA significantly increase relative to C-R2. These
726 changes signify a greater capacity for HCl absorption by organo-modified LDHs, as evidenced in the
727 MC-9OA compound. Thus, LDHs-2R-9OA not only reduces the rate of HCl release and diffusion but
728 also promotes enhanced HCl absorption with improved interactions with PVC. This discussion
729 elucidates the complex thermal degradation mechanisms of PVC and emphasizes the critical role of
730 OA in shaping interaction dynamics and thermal stabilization of LDHs. As the duration extends to
731 180 minutes, new peaks arise at 184 cm^{-1} and 160 cm^{-1} in Figure 16, corresponding to the formation
732 of $AlCl_3$ and $MgCl_2$, respectively (peak positions for $AlCl_3$ [83] and $MgCl_2$ [82] were both reported
733 in the literature). These changes signify a more pronounced interaction between LDHs and HCl, as
734 well as an increase in the polyene content within PVC structures. The findings of Raman spectroscopy
735 in this research are aligned with the prior investigations on the effectiveness of MgCaAlZn-LDH
736 [10]as a thermal stabilizer. They demonstrated that the cation can interact with HCl, which is produced
737 during the degradation of PVC, to form $MgCl_2$, $ZnCl_2$, $CaCl_2$, and $AlCl_3$.

738 Dehydrochlorination of PVC leads to the formation of polyene (Figure 17). The number of polyene
739 sequences can be calculated from the Raman spectra [84]:

740 $$\boldsymbol{v_2 = (1461 + 151.2 \times \exp(-0.7808 \times n))\ cm^{-1}}. \quad \textbf{(4)}$$

741 In this equation, the wavenumbers of the C=C stretching vibrations around 1500 cm^{-1} (Figure 16- b
742 and c) are designated as v_2, the length of polyenes is indicated as n, and the wavenumber of the C=C
743 stretching vibration is a function of n[85]. The findings are presented in Table 6, which
744 demonstrates that an elevation in temperature leads to an increase in the number of C=C bonds in
745 PVC chains and an increase in polyene length as shown in Figure 17. The results indicate that, after
746 10 minutes, the length of the polyene in both compounds falls within a similar range, whereas after
747 90 minutes, a significant disparity arises. Specifically, the length of the polyene ranges from 20-21
748 for CS-R2 and 12-13 for MC-9OA, respectively. Furthermore, based on the FTIR peaks (Figure S-9
749 and Figure S-10) the polyene index (PI) is determined utilizing [86]

750 $$\boldsymbol{PI = \frac{I_{1579}}{I_{2956}}\ or\ PI = \frac{I_{1600}}{I_{2956}}}. \quad \textbf{(5)}$$

The intensities of the FTIR peaks measured at 1579 cm^{-1} and 1600 cm^{-1} in PVC are denoted by I_{1579} and I_{1600}, respectively. These peaks correspond to the C=C bond vibrations in PVC. Meanwhile, the intensity of the peak observed at 2956 cm^{-1} in the PVC spectrum is represented by I_{2956} and signifies the presence of C-H bonds. The polyene index, a measure of the degree of C=C conjugated bonds in PVC, demonstrates a positive correlation with the intensities of both the 1579 cm^{-1} and 1600 cm^{-1} FTIR peaks. An increase in the intensities of the peaks at 1600 cm^{-1} and 1579 cm^{-1} indicates a greater abundance of C=C conjugated bonds and degradation of PVC. Therefore, PI can be measured using the intensity of either peak while the peak at 2956 cm^{-1} provides a reference. The results reveal that the rate of increase in PI matches the increasing length of polyenes, thereby confirming that the OA-modified LDH (MC-9OA) can better resist polyene formation in the thermal aging test than the unmodified (CS-R2).

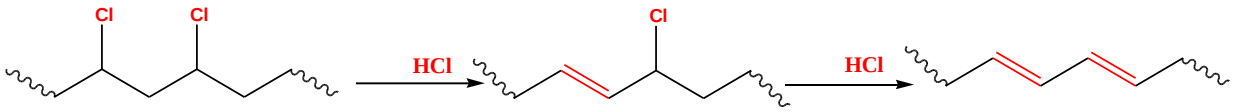

Figure 17 Mechanism of Polyene formation during the thermal degradation of PVC.

Table 6 Length of polyene and PI parameters of C-R2 and MC-9OA compounds.

Sample	Raman			FTIR	
	Peak	Area	n	P_{11579}	PI_{1600}
C-R2	-	-	-	0.0613	0.08348
MC-9OA	-	-	-	0.06567	0.08112
C-R2-10	1516	28.821	12.95	0.11935	0.12074
MC-9OA-10	1522	25.32	11.62	0.11606	0.12018
C-R2-90	1491	32.092	20.71	0.24328	0.24627
MC-9OA-90	1517	29.325	12.72	0.21769	0.22177
C-R2-180	1478	63.25	27.98	0.3	0.29225
MC-9OA-180	1485	48.680	23.57	0.23881	0.24328

4.5.2. Activation energy and Thermodynamic

To assess the impact of LDH surface modification on the activation energy in PVC degradation we used a non-isothermal technique. In these methods, the conversion of the degradation reaction is defined as[87]:

$$\boldsymbol{\alpha = \frac{m_o - m_i}{m_o - m_t}} \quad , \quad \textbf{(6)}$$

where m_o represents the original mass of the sample, m_i denotes the instantaneous mass at any time, and m_t signifies the final mass of the sample. The kinetic rate equation is expressed by the temperature-dependent rate constant, *k(T)*, and the temperature-independent reaction model, *f(X)*:

$$\frac{d\alpha}{dt} = k(T)f(\alpha) \quad (7)$$

The Arrhenius equation is used to describe the temperature dependence of reaction rates[88]:

$$k(T) = Aexp(-\frac{E_a}{RT}) \ . \quad (8)$$

where E_a is the activation energy. By substituting eq. (8) into eq. (7) and assuming a linear change of temperature – i.e., $T = T_0 + \beta t$, we get

$$\frac{d\alpha}{f(\alpha)} = \frac{A}{\beta}\exp\left(-\frac{E_a}{RT}\right)dT. \quad (9)$$

Integrating both sides of eq. (9) leads to

$$g(\alpha) = \int_0^{\alpha} \frac{d\alpha}{f(\alpha)} = \frac{A}{\beta}\int_0^{T} \exp\left(\frac{-E_a}{RT}\right)dT. \quad (10)$$

The function $g(\alpha)$ represents the integral conversion function. The integral on the right-hand side of eq. (10) lacks an exact analytical solution, but may be approximately evaluated to give:[89]

$$g(\alpha) = \frac{AR}{\beta E_a}T^2\left(1 - \frac{2RT}{E_a}\right)\exp\left(\frac{-E_a}{RT}\right). \quad (11)$$

Taking natural logarithm on both sides, we get a linearized form:

$$\boldsymbol{ln\left[\frac{g(\alpha)}{T^2}\right] = ln\left[\frac{AR}{\beta E_a}\left(1 - \frac{2RT}{E_a}\right)\right] - \frac{E_a}{RT}} \quad . \quad (12)$$

Equation (12) presents the Coats–Redfern method -- a non-isothermal model-fitting approach used to determine the kinetic parameters of solid-state materials[90] when the reaction temperature increases

at a constant rate[91]. Assuming that the $\frac{2RT}{E_a}$ term is much less than 1, we can neglect the factor in parentheses, resulting in the modified equation[90]:

$$\boldsymbol{ln}\left[\frac{\boldsymbol{g(\alpha)}}{\boldsymbol{T^2}}\right] = \boldsymbol{ln}\left[\frac{\boldsymbol{AR}}{\boldsymbol{\beta E_a}}\right] - \frac{\boldsymbol{E_a}}{\boldsymbol{RT}} \quad . \qquad (13)$$

The parameter β denotes the heating rate (°C/min) and A is called the frequency factor (min^{-1}). The ideal gas constant, R, has a value of 8.3143 J/mol·K.

By plotting $ln\left[\frac{g(\alpha)}{T^2}\right]$ against $1/T$, we determined both the activation energy E_a and the frequency factor A from the slope ($-E_a/R$) and intercept $ln\left[\frac{AR}{\beta E_a}\right]$ of the resulting linear relationship [92] . The function g(α) varies depending on the kinetics model. In this research we considered $g(\alpha) = -\ln(1-\alpha)$ for the first-order reaction in the PVC degradation process. The analysis was performed during the two TGA mass-loss stages identified in previous sections for PVC compounds (Figure 15-a), and at the temperature corresponding to the maximum rate of mass loss T_{Max} and T_{onset} for each stage.

Figure S-11 shows the effect of LDHs on sample stability and thermal degradation, using conversion vs. temperature based on the TGA results in Figure 15-a. All samples show a sigmoidal conversion curve, but MC-9OA starts degrading at a lower temperature due to the absorption of small molecules and unreacted OA on the LDH surface. As the temperature rises, CS degrades faster than C-R2 and MC-9OA. At 30% conversion, MC-9OA shifts to higher temperatures, indicating slower degradation. At 50% conversion, the temperatures for CS, C-R2, and MC-9OA are 288°C, 299°C, and 311°C, respectively. Furthermore, the plots of the differential conversion rate (dα/dT) as a function of temperature (Figure S-12) confirm that OA potentially serves as a barrier to the migration of deleterious polar factors within the system.

The activation energy was measured for the two degradation stages observed in TGA for CS, CR-2, and MC-9OA samples. When LDH was incorporated into PVC compounds, the activation energy in stage I increased from 145 to 152.8 kJ/mol for CS and CR-2, respectively. This indicates that the degradation of PVC requires more energy in the presence of LDH. Moreover, the organo-modified LDH had a contributing effect on the activation energy, leading to an increase to 158.56 kJ/mol. This suggests that OA enhances the thermal stability efficiency of LDH, reduces the presence of HCl, and eliminates its catalytic effect. In stage II, the activation energy was 257.76**kJ/mol**, 229.87**kJ/mol**, and 258.78**kJ/mol** for CS, CR-2, and MC-9OA, respectively. This behavior signifies the emergence of reactions that culminate in the creation of more enduring structures, including stable residues and

polyene compounds[93]. These structures are generated after the dehydrochlorination process, wherein decomposition transpires and robust structures such as aromatic and graphitic structures come into existence[94]. Finally, the average activation energy calculated in this study for pure PVC dehydrochlorination (145 kJ/mol) completely matches the value reported by Zhou et al. [90](145.33 kJ/mol) using the CR model. This confirms the validity of the procedure used to calculate the kinetic data.

5. Conclusion

In this study, a MgAlZn-CO_3 ternary LDH material was synthesized and its effectiveness as a thermal stabilizer for PVC compounding was evaluated. The Mg/Zn ratio *R* was optimized for the best PVC stabilization performance. The LDH with the optimal $R = 2$ was used as a base material for surface modification by OA. OA was shown to have a significant influence on the crystal structure and the surface chemistry of LDHs. When a higher ratio of OA to LDHs was employed, OA enhanced the crystallinity of LDHs and reduced the surface energy, leading to more stable LDHs. Additionally, in the presence of OA, the compatibility of LDHs was greatly improved compared to unmodified LDHs, resulting in a uniform distribution and high dispersity of LDHs in PVC. Furthermore, the incorporation of OA in LDHs decreased the auto-catalytic effect of PVC degradation with HCl reduction. The discoloration results revealed that as the Mg/Zn ratio increased, the color stability decreased in the initial stages of degradation. However, the long-term thermal stability improved. In the presence of OA, color stability of the PVC compound further improved compared with those using unmodified LDHs, and the modified compounds did not turn black after 180 minutes under 180 °C thermal aging conditions. Furthermore, with the presence of OA, the thermal degradation shifted to a higher temperature, and the intensity of weight loss decreased. Raman spectroscopy demonstrated that under thermal aging conditions, LDHs absorbed HCl and formed metal chlorides ($MgCl_2$, $ZnCl_2$, and $AlCl_3$). The area and intensity of the assigned peaks increased with time, indicating the high capacity of LDHs to absorb HCl. Polyene chains, which are degradation products, gradually increase in length over time. However, polyene formation is notably reduced with OA-modified LDHs.

This study demonstrated that OA shows great promise as a new, environmentally friendly modifier to improve the compatibility of LDHs with PVC matrix and enhance their thermal stabilization performance. OA-modified LDHs show great potential as a competitive new thermal stabilizer for general PVC compounding as well as for PVC recycling and reprocessing. In particular, thermal stability is a critical factor in the mechanical reprocessing of PVC and in building a circular vinyl

economy at large. Continued research will explore the application of OA-modified LDHs in PVC reprocessing technologies.

Acknowledgments

This work was supported by the Natural Sciences and Engineering Research Council of Canada (NSERC) Alliance Missions Grant (No. ALLRP -570505-2021). Support to this work from Oligomaster Inc. (Hamilton, ON, Canada) and Pixiu Solutions Inc (Brantford, ON, Canada) is also acknowledged. Generous donation of materials from Shintech Inc., Evonik Oxeno LLC, Clarient Specialty Chemicals, and AM Stabilizers is greatly appreciated.

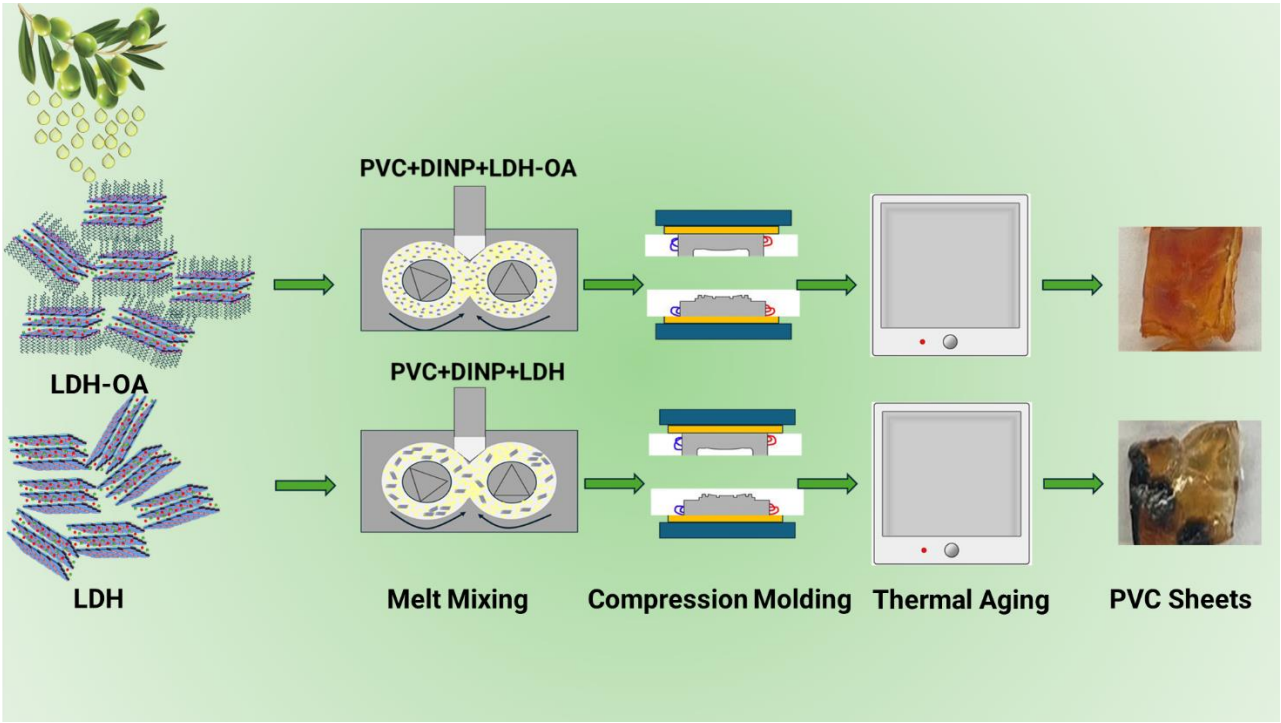

6. References

[1] Lewandowski K, Skórczewska K. A Brief Review of Poly(Vinyl Chloride) (PVC) Recycling. Polymers. 2022;14(15):3035.

[2] Bhunia K, Sablani SS, Tang J, Rasco B. Migration of chemical compounds from packaging polymers during microwave, conventional heat treatment, and storage. comprehensive Reviews in food Science and food Safety. 2013;12(5):523-45.

[3] Ahmad N, Kausar A, Muhammad B. Perspectives on polyvinyl chloride and carbon nanofiller composite: a review. Polymer-Plastics Technology and Engineering. 2016;55(10):1076-98.

[4] Hazer B, Karahaliloglu Z, Ashby RD. Poly (vinyl chloride) derived food packaging applications with Antioxidative and Anticancer properties. ACS Food Science & Technology. 2023;3(4):761-71.

[5] K J A, M M. Application of PVC – A superior material in the fields of Science and Technology. Polymer-Plastics Technology and Materials.1-19.

[6] Chiellini F, Ferri M, Morelli A, Dipaola L, Latini G. Perspectives on alternatives to phthalate plasticized poly (vinyl chloride) in medical devices applications. Progress in polymer science. 2013;38(7):1067-88.

[7] Cruz PPR, da Silva LC, Fiuza-Jr RA, Polli H. Thermal dehydrochlorination of pure PVC polymer: Part I—thermal degradation kinetics by thermogravimetric analysis. Journal of Applied Polymer Science. 2021;138(25):50598.

[8] Babinsky R. PVC additives: A global review. Plastics, Additives and Compounding. 2006;8(1):38-40.

[9] Jaishankar M, Tseten T, Anbalagan N, Mathew B, Beeregowda K. Toxicity, mechanism and health effects of some heavy metals. Interdiscip Toxicol 7: 60–72. 2014.

[10] Guo Y, Leroux F, Tian W, Li D, Tang P, Feng Y. Layered double hydroxides as thermal stabilizers for Poly(vinyl chloride): A review. Applied Clay Science. 2021;211:106198.

[11] chemanalyst. Production, Operating Efficiency, Demand & Supply, End-User Industries, Sales Channel, Regional Demand, Foreign Trade, Company Share, Manufacturing Process, 2015-2030. chemanalyst; 2023.

[12] Wang Q, O'Hare D. Recent Advances in the Synthesis and Application of Layered Double Hydroxide (LDH) Nanosheets. Chemical Reviews. 2012;112(7):4124-55.

[13] Van der Ven L, Van Gemert M, Batenburg L, Keern J, Gielgens L, Koster T, et al. On the action of hydrotalcite-like clay materials as stabilizers in polyvinylchloride. Applied Clay Science. 2000;17(1-2):25-34.

[14] Bukhtiyarova MV. A review on effect of synthesis conditions on the formation of layered double hydroxides. Journal of Solid State Chemistry. 2019;269:494-506.

[15] Lin Y-J, Li D-Q, Evans DG, Duan X. Modulating effect of Mg–Al–CO3 layered double hydroxides on the thermal stability of PVC resin. Polymer Degradation and Stability. 2005;88(2):286-93.

[16] Mallakpour S, Hatami M. Biosafe organic diacid intercalated LDH/PVC nanocomposites versus pure LDH and organic diacid intercalated LDH: synthesis, characterization and removal behaviour of Cd2+ from aqueous test solution. Applied Clay Science. 2017;149:28-40.

[17] Zhang X, Zhao T, Pi H, Guo S. Preparation of intercalated Mg‐Al layered double hydroxides and its application in PVC thermal stability. Journal of applied polymer science. 2012;124(6):5180-6.

[18] Aisawa S, Nakada C, Hirahara H, Takahashi N, Narita E. Preparation of dipentaerythritol-combined layered double hydroxide particle and its thermostabilizing effect for polyvinyl chloride. Applied Clay Science. 2019;180:105205.

[19] Yan J, Yang Z. Intercalated hydrotalcite‐like materials and their application as thermal stabilizers in poly (vinyl chloride). Journal of Applied Polymer Science. 2017;134(22).
[20] Liu J, Chen G, Yang J, Ding L. Improved thermal stability of poly(vinyl chloride) by nanoscale layered double hydroxide particles grafted with toluene-2,4-di-isocyanate. Materials Chemistry and Physics. 2009;118(2):405-9.
[21] Liu J, Chen G, Yang J. Preparation and characterization of poly (vinyl chloride)/layered double hydroxide nanocomposites with enhanced thermal stability. Polymer. 2008;49(18):3923-7.
[22] Mei X, Jiang P, Zhang P, Cui Z, Zhu X, Chen S, et al. Enhancing mechanical properties of polyvinyl chloride: Novel organic‐modified cinnamate‐intercalated calcium aluminum hydrotalcite as a high‐efficiency thermal stabilizer. Journal of Vinyl and Additive Technology. 2024.
[23] Bao YZ, Huang ZM, Weng ZX. Preparation and characterization of poly (vinyl chloride)/layered double hydroxides nanocomposite via in situ suspension polymerization. Journal of applied polymer science. 2006;102(2):1471-7.
[24] Liu J, Chen G, Yang J, Ding L. Improved thermal stability of poly (vinyl chloride) by nanoscale layered double hydroxide particles grafted with toluene-2, 4-di-isocyanate. Materials Chemistry and Physics. 2009;118(2-3):405-9.
[25] Choi S-G, Won S-R, Rhee H-I. Chapter 153 - Oleic Acid and Inhibition of Glucosyltransferase. In: Preedy VR, Watson RR, editors. Olives and Olive Oil in Health and Disease Prevention. San Diego: Academic Press; 2010. p. 1375-83.
[26] Wen J-x, Xie Z-p, Cao W-b. Novel fabrication of more homogeneous water-soluble binder system feedstock by surface modification of oleic acid. Ceramics International. 2016;42(14):15530-5.
[27] Obata H. Preparation of oleate/layered double hydroxides (LDHs) composites from LDHs with different porous properties and its acid-resistant properties. Abstracts of 50th Clay Science Society of Japan, 2006. 2006:186-7.
[28] Zhonghui L, Guida S. Factors Affecting Acidity and Basal Spacing of Cross-Linked Smectites. In: Držaj B, Hočevar S, Pejovnik S, editors. Studies in Surface Science and Catalysis: Elsevier; 1985. p. 493-500.
[29] Gevers BR, Naseem S, Leuteritz A, Labuschagné FJWJ. Comparison of nano-structured transition metal modified tri-metal MgMAl–LDHs (M = Fe, Zn, Cu, Ni, Co) prepared using co-precipitation. RSC Advances. 2019;9(48):28262-75.
[30] Bhattacharjee S. Synthesis and application of layered double hydroxide-hosted 2-aminoterephthalate for the Knoevenagel condensation reaction. Inorganic and Nano-Metal Chemistry. 2018;48(7):340-6.
[31] Nejati K, Akbari AR, Davari S, Asadpour-Zeynali K, Rezvani Z. Zn–Fe-layered double hydroxide intercalated with vanadate and molybdate anions for electrocatalytic water oxidation. New Journal of Chemistry. 2018;42(4):2889-95.
[32] Evans DG, Slade RC. Structural aspects of layered double hydroxides. Layered double hydroxides. 2006:1-87.
[33] Evans DG, Slade RCT. Structural Aspects of Layered Double Hydroxides. In: Duan X, Evans DG, editors. Layered Double Hydroxides. Berlin, Heidelberg: Springer Berlin Heidelberg; 2006. p. 1-87.
[34] Riahi S, Roux B, Rowley CN. QM/MM molecular dynamics simulations of the hydration of Mg (II) and Zn (II) ions. Canadian Journal of Chemistry. 2013;91(7):552-8.
[35] Zhang X, Zhou L, Pi H, Guo S, Fu J. Performance of layered double hydroxides intercalated by a UV stabilizer in accelerated weathering and thermal stabilization of PVC. Polymer Degradation and Stability. 2014;102:204-11.

[36] Sakr AAE, Zaki T, Elgabry O, Ebiad MA, El-Sabagh SM, Emara MM. Mg-Zn-Al LDH: Influence of intercalated anions on CO2 removal from natural gas. Applied Clay Science. 2018;160:263-9.
[37] Valeikiene L, Paitian R, Grigoraviciute-Puroniene I, Ishikawa K, Kareiva A. Transition metal substitution effects in sol-gel derived Mg3-xMx/Al1 (M = Mn, Co, Ni, Cu, Zn) layered double hydroxides. Materials Chemistry and Physics. 2019;237:121863.
[38] Labuschagne FJWJ, Molefe DM, Focke WW, van der Westhuizen I, Wright HC, Royeppen MD. Heat stabilising flexible PVC with layered double hydroxide derivatives. Polymer Degradation and Stability. 2015;113:46-54.
[39] Karami Z, Jouyandeh M, Ali JA, Ganjali MR, Aghazadeh M, Maadani M, et al. Development of Mg-Zn-Al-CO3 ternary LDH and its curability in epoxy/amine system. Progress in Organic Coatings. 2019;136:105264.
[40] Naseem S, Gevers B, Boldt R, Labuschagné FJW, Leuteritz A. Comparison of transition metal (Fe, Co, Ni, Cu, and Zn) containing tri-metal layered double hydroxides (LDHs) prepared by urea hydrolysis. RSC advances. 2019;9(6):3030-40.
[41] Rahman N, Raheem A. Graphene oxide/Mg-Zn-Al layered double hydroxide for efficient removal of doxycycline from water: Taguchi approach for optimization. Journal of Molecular Liquids. 2022;354:118899.
[42] Labuschagné J, Molefe D, Focke WW, Ofosu O. Layered Double Hydroxide Derivatives as Flame Retardants for Flexible PVC. Macromolecular Symposia. 2019;384(1):1800148.
[43] Zhou X, Chen H, Chen Q, Ling Q. Synthesis and characterization of two-component acidic ion intercalated layered double hydroxide and its use as a nanoflame-retardant in ethylene vinyl acetate copolymer (EVA). RSC Advances. 2017;7(84):53064-75.
[44] Klempová S, Oravec M, Vizárová K. Analysis of thermally and UV–Vis aged plasticized PVC using UV–Vis, ATR-FTIR and Raman spectroscopy. Spectrochimica Acta Part A: Molecular and Biomolecular Spectroscopy. 2023;294:122541.
[45] Yaseen AA, Yousif E, Al-Tikrity ETB, El-Hiti GA, Kariuki BM, Ahmed DS, et al. FTIR, Weight, and Surface Morphology of Poly(vinyl chloride) Doped with Tin Complexes Containing Aromatic and Heterocyclic Moieties. Polymers. 2021;13(19):3264.
[46] Pandey M, Joshi GM, Mukherjee A, Thomas P. Electrical properties and thermal degradation of poly(vinyl chloride)/polyvinylidene fluoride/ZnO polymer nanocomposites. Polymer International. 2016;65(9):1098-106.
[47] Ul-Hamid A, Soufi KY, Al-Hadhrami LM, Shemsi AM. Failure investigation of an underground low voltage XLPE insulated cable. Anti-Corrosion Methods and Materials. 2015;62(5):281-7.
[48] Rao Z, Li K, Liu P, Lin Y, Lyu X. Study on the Thermal Stabilizing Process of Layered Double Hydroxides in PVC Resin. Molecules. 2023;28(23):7792.
[49] Cui C, Zhang Y, Wladyka MA, Wang T, Song W, Niu K. Ultrasound-Assisted Adsorption of Perchlorate Using Calcined Hydrotalcites and the Thermal Stabilization Effect of Recycled Adsorbents on Poly(vinyl chloride). ACS Omega. 2023;8(20):17689-98.
[50] Guo Y, Zhang Q, Hu Q, Tian W, Leroux F, Tang P, et al. Size-dependent effect of MgAl-layered double hydroxides derived from Mg(OH)2 on thermal stability of poly(vinyl chloride). Materials Today Communications. 2021;29:102851.
[51] Wang G, Yang M, Li Z, Lin K, Jin Q, Xing C, et al. Synthesis and characterization of Zn-doped MgAl-layered double hydroxide nanoparticles as PVC heat stabilizer. Journal of nanoparticle research. 2013;15:1-8.
[52] Zhang H-m, Zhang S-h, Stewart P, Zhu C-h, Liu W-j, Hexemer A, et al. Thermal stability and thermal aging of poly (vinyl chloride)/MgAl layered double hydroxides composites. Chinese Journal of Polymer Science. 2016;34:542-51.

[53] Dong T, Li D, Li Y, Han W, Zhang L, Xie G, et al. Design and synthesis of polyol ester-based zinc metal alkoxides as a bi-functional thermal stabilizer for poly (vinyl chloride). Polymer Degradation and Stability. 2019;159:125-32.
[54] Yu J, Sun L, Ma C, Qiao Y, Yao H. Thermal degradation of PVC: A review. Waste Management. 2016;48:300-14.
[55] Wypych G. Stabilization and stabilizers. Handbook of Material Weathering. 2013;6:785-827.
[56] Yan J, Yang Z. Intercalated hydrotalcite-like materials and their application as thermal stabilizers in poly(vinyl chloride). Journal of Applied Polymer Science. 2017;134(22).
[57] Wang H, Li C, Geng T, Du N, Hou W. Oleic acid-modified layered double hydroxide for Pickering emulsion: (II) Emulsification behavior. Colloids and Surfaces A: Physicochemical and Engineering Aspects. 2024;687:133568.
[58] Haarindraprasad R, Hashim U, Gopinath SC, Kashif M, Veeradasan P, Balakrishnan S, et al. Low temperature annealed zinc oxide nanostructured thin film-based transducers: characterization for sensing applications. PLoS One. 2015;10(7):e0132755.
[59] Zhang P, He T, Li P, Zeng X, Huang Y. New Insight into the Hierarchical Microsphere Evolution of Organic Three-Dimensional Layer Double Hydroxide: The Key Role of the Surfactant Template. Langmuir. 2019;35(42):13562-9.
[60] Zhang Q, Zhang G, Huang Y, He S, Li Y, Jin L, et al. Surface-Modified LDH Nanosheets with High Dispersibility in Oil for Friction and Wear Reduction. ACS Applied Materials & Interfaces. 2024;16(4):5316-25.
[61] Kameshima Y, Sasaki H, Isobe T, Nakajima A, Okada K. INTERCALATION BEHAVIOR OF VARIOUS FATTY ACIDS INTO Mg-Al-LAYERED DOUBLE HYDROXIDE. Clay Science. 2009;14(2):87-94.
[62] Lee DH, Condrate RA, Lacourse WC. FTIR spectral characterization of thin film coatings of oleic acid on glasses Part II Coatings on glass from different media such as water, alcohol, benzene and air. Journal of Materials Science. 2000;35(19):4961-70.
[63] Shukla N, Liu C, Jones PM, Weller D. FTIR study of surfactant bonding to FePt nanoparticles. Journal of Magnetism and Magnetic Materials. 2003;266(1):178-84.
[64] Shorey R, Mekonnen TH. Oleic acid decorated kraft lignin as a hydrophobic and functional filler of cellulose acetate films. International Journal of Biological Macromolecules. 2024;268:131672.
[65] Lei X, Lu W, Peng Q, Li H, Chen T, Xu S, et al. Activated MgAl-layered double hydroxide as solid base catalysts for the conversion of fatty acid methyl esters to monoethanolamides. Applied Catalysis A: General. 2011;399(1):87-92.
[66] Dibenedetto CN, Sibillano T, Brescia R, Prato M, Triggiani L, Giannini C, et al. PbS Quantum Dots Decorating TiO2 Nanocrystals: Synthesis, Topology, and Optical Properties of the Colloidal Hybrid Architecture. Molecules. 2020;25(12):2939.
[67] Fa K, Jiang T, Nalaskowski J, Miller JD. Optical and Spectroscopic Characteristics of Oleate Adsorption As Revealed by FTIR Analysis. Langmuir. 2004;20(13):5311-21.
[68] Tang Z-H, Zeng H-Y, Zhang K, Yue H-L, Tang L-Q, Lv S-B, et al. Engineering core–shell NiC2O4@C/N-direct-doped NiCoZn-LDH for supercapacitors. Chemical Engineering Science. 2024;289:119865.
[69] Chen Y, Wu L, Yao W, Wu J, Xie Z, Yuan Y, et al. In situ growth of Mg-Zn-Al LDHs by ZIF-8 carrying Zn source and micro-arc oxidation integrated coating for corrosion and protection of magnesium alloys. Surface and Coatings Technology. 2022;451:129032.
[70] Zhao J, Lu Y, Wu D, Qin Y, Xie Y, Guo Y, et al. Regulating divalent metal species in aluminum-based layered double hydroxides to selectively promote photocatalytic CO production from CO2. Separation and Purification Technology. 2023;305:122508.
[71] Kotal M, Srivastava SK. Synergistic effect of organomodification and isocyanate grafting of layered double hydroxide in reinforcing properties of polyurethane nanocomposites. Journal of Materials Chemistry. 2011;21(46):18540-51.

[72] Xu ZP, Braterman PS, Yu K, Xu H, Wang Y, Brinker CJ. Unusual Hydrocarbon Chain Packing Mode and Modification of Crystallite Growth Habit in the Self-Assembled Nanocomposites Zinc−Aluminum-Hydroxide Oleate and Elaidate (cis-and trans-[Zn2Al (OH) 6 (CH3 (CH2) 7CH CH (CH2) 7COO-)] and Magnesium Analogues. Chemistry of materials. 2004;16(14):2750-6.
[73] Xu Z, Zeng H. Decomposition Processes of Organic-Anion-Pillared Clays Co a Mg b Al (OH) c (TA) d⊙ n H2O. The Journal of Physical Chemistry B. 2000;104(44):10206-14.
[74] Bajwa DS, Rehovsky C, Shojaeiarani J, Stark N, Bajwa S, Dietenberger MA. Functionalized cellulose nanocrystals: A potential fire retardant for polymer composites. Polymers. 2019;11(8):1361.
[75] Yang H, Yang Z. The effect of sodium stearate-modified hydrocalumite on the thermal stability of poly(vinyl chloride). Journal of Applied Polymer Science. 2018;135(4):45758.
[76] Li M, Zhang J, Huang K, Li S, Jiang J, Xia J. Mixed calcium and zinc salts of dicarboxylic acids derived from rosin and dipentene: preparation and thermal stabilization for PVC. RSC Advances. 2014;4(108):63576-85.
[77] Li M, Zhang J, Xin J, Huang K, Li S, Wang M, et al. Design of green zinc-based thermal stabilizers derived from tung oil fatty acid and study of thermal stabilization for PVC. Journal of Applied Polymer Science. 2017;134(14).
[78] Li Y, Li D, Han W, Zhang M, Ai B, Zhang L, et al. Facile Synthesis of Di-Mannitol Adipate Ester-Based Zinc Metal Alkoxide as a Bi-Functional Additive for Poly(Vinyl Chloride). Polymers. 2019;11(5):813.
[79] Babushkina OB, Volkov SV. Raman spectroscopy of the heteronuclear complexes in the ZnCl2 · CdCl2 · Li,K/Cl and AlCl3 · MgCl2 · Li,K/Cl melts. Journal of Molecular Liquids. 1999;83(1):131-40.
[80] Alsayoud AQ, Venkateswara Rao M, Edwards AN, Deymier PA, Muralidharan K, Potter BG, Jr., et al. Structure of ZnCl2 Melt. Part I: Raman Spectroscopy Analysis Driven by Ab Initio Methods. The Journal of Physical Chemistry B. 2016;120(17):4174-81.
[81] Zhang X, Li S, Yuan J, Shi Z. Influence of magnesium chloride on the electrodeposition of zinc from the 1,3-dimethyl-2-imidazolidinone/ZnCl2 system. Journal of Electroanalytical Chemistry. 2024;957:118131.
[82] Sano H, Miyaoka H, Kuze T, Mori H, Mizutani G, Otsuka N, et al. Raman spectra of magnesium chloride thin films. Surface Science. 2002;502-503:70-4.
[83] Begun GM, Brynestad J, Fung KW, Mamantov G. Raman spectra of the molten AlCl3 · ZnCl2 system and molten Cs2ZnCl4. Inorganic and Nuclear Chemistry Letters. 1972;8(1):79-88.
[84] Kuznetsov SM, Sagitova EA, Prokhorov KA, Nikolaeva GY, Mendeleev DI, Donfack P, et al. Raman spectroscopic detection of polyene-length distribution for high-sensitivity monitoring of photo- and thermal degradation of polyvinylchloride. Spectrochimica Acta Part A: Molecular and Biomolecular Spectroscopy. 2021;252:119494.
[85] Gilbert M, Ho KC, Hitt DJ, Vrsaljko D. Assessment of PVC stabilisation using hydrotalcites – Raman spectroscopy and other techniques. Polymer Degradation and Stability. 2013;98(8):1537-47.
[86] Saeedi M, Ghasemi I, Karrabi M. Thermal degradation of poly (vinyl chloride): effect of nanoclay and low density polyethylene content. 2011.
[87] Sánchez-Jiménez PE, Pérez-Maqueda LA, Perejón A, Criado JM. Combined kinetic analysis of thermal degradation of polymeric materials under any thermal pathway. Polymer Degradation and Stability. 2009;94(11):2079-85.
[88] Wang Z, Xie T, Ning X, Liu Y, Wang J. Thermal degradation kinetics study of polyvinyl chloride (PVC) sheath for new and aged cables. Waste Management. 2019;99:146-53.
[89] Coats AW, Redfern JP. Kinetic Parameters from Thermogravimetric Data. Nature. 1964;201(4914):68-9.
[90] Zhou R, Huang B, Ding Y, Li W, Mu J. Thermal Decomposition Mechanism and Kinetics Study of Plastic Waste Chlorinated Polyvinyl Chloride. Polymers. 2019;11(12):2080.

[91] Raza M, Abu-Jdayil B, Al-Marzouqi AH, Inayat A. Kinetic and thermodynamic analyses of date palm surface fibers pyrolysis using Coats-Redfern method. Renewable Energy. 2022;183:67-77.
[92] Rami JM, Patel CD, Patel CM, Patel MV. Thermogravimetric analysis (TGA) of some synthesized metal oxide nanoparticles. Materials Today: Proceedings. 2021;43:655-9.
[93] Gao H, Li J. Thermogravimetric analysis of the co-combustion of coal and polyvinyl chloride. Plos one. 2019;14(10):e0224401.
[94] Jordan KJ, Suib SL, Koberstein JT. Determination of the Degradation Mechanism from the Kinetic Parameters of Dehydrochlorinated Poly(vinyl chloride) Decomposition. The Journal of Physical Chemistry B. 2001;105(16):3174-81.